Phenolic furanochromene hydrazone derivatives: **Synthesis, antioxidant activity, ferroptosis inhibition, DNA cleavage and DNA molecular docking studies**

Jessica L. Saylor,[a]# Olivia N. Basile,[a]# Huifang Li,[b] Lindsey M. Hunter,[a] Ashton Weaver,[a] Blake M. Shellenberger,[a] Lou Ann Tom,[a] Hang Ma,[b] Navindra P. Seeram,[b] Geneive E. Henry[a*]

[a]*Department of Chemistry, Susquehanna University, 514 University Avenue, Selinsgrove, PA 17870, USA*

[b]*Bioactive Botanical Research Laboratory*, *Department of Biomedical and Pharmaceutical Sciences, College of Pharmacy, University of Rhode Island, Kingston, RI 02881, USA*

#These authors contributed equally to the work.

***Corresponding author:**

Geneive E. Henry

Department of Chemistry, Susquehanna University, 514 University Avenue, Selinsgrove, PA 17870

Telephone: 570-372-4222

E-mail: henry@susqu.edu

HIGHLIGHTS

- Synthesis of phenolic furanochromene hydrazone derivatives.
- Derivatives with *ortho*-dihydroxy groups showed strong DPPH free radical scavenging and copper (II) ion reducing activities.
- More than half of the furanochromene derivatives exhibited ferroptosis inhibitory activity.
- The derivatives cleaved plasmid DNA and showed strong binding affinity to DNA through molecular docking studies.

ABSTRACT

A series of twenty-four phenolic furanochromene hydrazone derivatives (**11a-11x**) were synthesized, with varying substitution pattern on the phenol ring. Half of the compounds contain one, two or three hydroxy groups on the phenol ring, while the other half contain one hydroxy in combination with methoxy, methyl, bromo, iodo and/or nitro groups. Several assays were performed to determine the influence of the nature and location of the substituents on biological activities. Antioxidant potential was determined using the DPPH free radical scavenging and CUPRAC assays. Compounds **11a-11b**, **11d-11e** and **11g-11h,** which contain *ortho*-dihydroxy groups or *para*-dihydroxy groups, had the highest free radical scavenging activity, with IC_{50} values ranging from 5-28 μM. A similar pattern was observed for the CUPRAC assay, with compounds **11a-11b**, **11d** and **11h** displaying strong copper (II) reducing capacity, using Trolox as a standard. Trolox equivalent antioxidant capacity (TEAC) coefficients for these derivatives ranged from 2.43 to 3.97. As further evidence of antioxidant potential, greater than half of the derivatives reversed erastin-induced ferroptosis in HaCaT cells, with derivatives **11a** and **11g** being the most effective. In addition, twenty-three of the derivatives were effective at cleaving plasmid DNA in the presence of copper (II) ions at 1 mM, with 3,4-dihydroxy derivative **11h** showing cleavage to both the linear and open circular forms at 3.9 uM. The interaction of the phenolic furanochromene derivatives with DNA was confirmed by molecular docking studies, which indicated strong binding affinity with docking scores of -9.5 to -10.9 kcal/mol.

Keywords: Phenolic furanochromene hydrazones; Antioxidant; Anti-ferroptosis; DNA cleavage; DNA molecular docking

1. INTRODUCTION

The heterocyclic 2,2-dimethyl-2*H*-chromene (2,2-dimethylbenzopyran) moiety is present in many plant-derived natural products and imparts a diverse range of biological activities to these compounds, including anticancer, antimicrobial, anti-HIV, anti-inflammatory, and antioxidant effects.[1-2] Many of these chromene derivatives contain a second or third heterocyclic ring fused to the benzene ring. Among this class of compounds, those which contain an additional pyran or pyranone ring, or their dihydro equivalent, are most prevalent.[3-9] Two important examples are deguelin (**1**) and calanolide A (**2**) (Fig. 1), isolated from *Mundulea sericea* and *Calophyllum lanigerum*, respectively. Deguelin has shown anticancer activity against a wide range of cancer cell types,[10] and calanolide A is effective against HIV-I reverse transcriptase.[11] Owing to their potency, both compounds have been used in preclinical studies and clinical trials.[10,12]

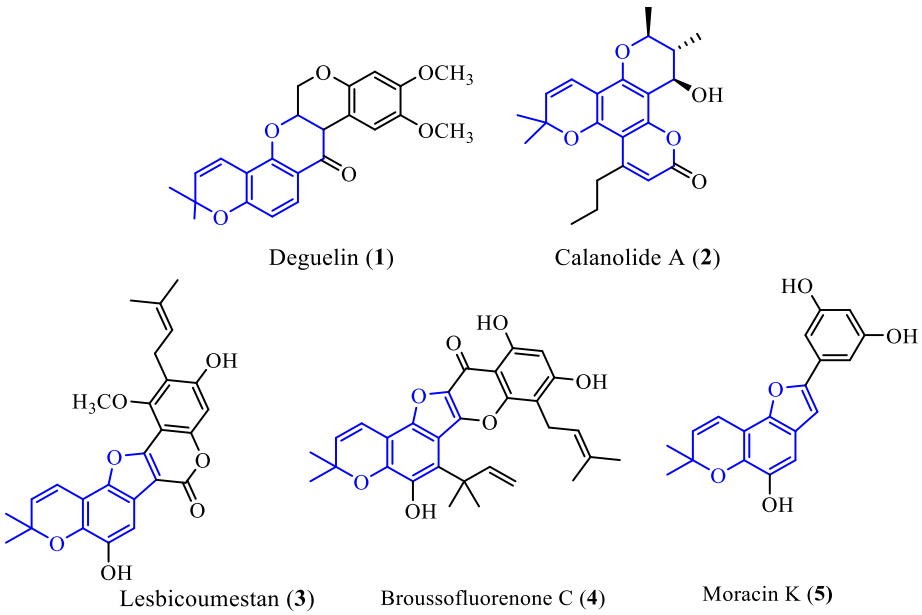

Fig. 1. Biologically active pyranochromene and furanochromene derivatives

In contrast, furanochromene derivatives which contain a furan ring fused to the chromene benzene ring are less common. Examples include the angular phenolic furanochromenes,

lesbicoumestan (**3**), broussofluorenone C (**4**) and moracin K (**5**) (Fig. 1). Lesbicoumestan is an anticancer compound that was isolated from *Lespedeza bicolor*.[13-14] Broussofluorenone C was isolated from *Broussonetia papyrifera*, and exhibits both antioxidant and anti-inflammatory activities.[15] Moracin K is one of over two dozen aryl benzofurans from the *Morus* genus, and was isolated from *Morus mesozygia*.[16] Although several moracins from various *Morus* species have demonstrated anticancer, antioxidant and anti-Alzheimer's activity, [17-19] to our knowledge, there is no reported biological activity for moracin K, which is one of the few moracins containing a chromene moiety.

Given the biological activities associated with naturally occurring 2,2-dimethyl chromene derivatives, there has been a strong interest in developing synthetic derivatives with enhanced pharmacological profiles. Toward this goal, several derivatives of both deguelin[20-21] and calanolide A,[22-23] together with other pyranochromenes,[24-25] have been synthesized. However, there have been fewer reports of synthetic furanochromene derivatives, which includes a set of modified calanolide A derivatives.[22] Recently, a series of furanochromene chalcones was developed as inhibitors of anoctamin 1 (ANO1).[26] In addition, Boddupally et al[27] and Ashok et al,[28] developed a series of antimicrobial furanochromenes, in which the two methyl groups at C-2 on the pyran ring are missing. Given the dearth of synthetic furanochromene derivatives and assessment of biological activities, there is value in expanding the literature on this class of compounds.

Reactive oxygen species (ROS) are produced in the body as a part of normal metabolism. Endogenous antioxidants help to balance the amount of ROS, leading to redox homeostasis. Oxidative stress occurs when there is an excess of ROS, which can damage biomolecules such as DNA, proteins and lipids, and cause cardiovascular disease, neurodegenerative disorders and cancers.[29-30] One of the mechanisms by which ROS is produced is redox cycling by the reduction

and subsequent oxidation of redox active iron and copper ions by cellular oxidants. This mechanism is associated with ferroptosis, a regulated form of cell death that was discovered a decade ago. Ferroptosis is iron-dependent and leads to the accumulation of lipid peroxides.[31] Oxidative stress-induced cell damage, including ferroptosis, can be alleviated by exogenous antioxidants, which may exert cytoprotective effects in normal cells.

The most prevalent class of exogenous antioxidants includes phenol-containing compounds, which exhibit their antioxidant activity primarily by scavenging free radicals.[29-30, 32-33] In addition, they play a role in chelating redox active iron and copper ions and/or reducing them, and thus can function as anti-ferroptotic agents.[34-35] Furthermore, in the presence of cancer cells, which have a high concentration of these metal ions, phenols can act as prooxidants, increasing ROS levels.[36-37] Thus, phenols can be used to selectively target biomolecules in cancer cells, leading to cell death. Because of its role in controlling cellular functions, DNA is a target of many anticancer drugs, and oxidative damage of DNA as a result of ROS generated by redox cycling can be used as an indicator of anticancer potential.[37-39]

Molecular hybridization, which involves the combination of two or more bioactive units into a single molecule, is a common strategy in drug design.[40] Inspired by the pharmacological profiles of furanochromenes and phenolic compounds, we aim to synthesize a series of moracin K-like furanochromene-phenolic hybrid compounds, containing a bioactive hydrazone linker. The *N*-acyl-hydrazone moiety (-CO-NH-N=CH-) has been incorporated in hundreds of synthetic molecules, and a survey of the literature indicates that it plays a role in a myriad of biological activities.[41-44] This strategy of linking a phenolic ring to a heterocyclic bioactive moiety via an *N*-acyl hydrazone to develop compounds with potential antioxidant and anticancer properties has previously been employed by Baldisserotto et al.[45-47] However, to our knowledge this is the first report linking a furanochromene to a phenolic moiety via an *N*-acyl-hydrazone linker.

The designed furanochromene-hydrazone hybrids are divided into two main series, depending on the substitution on the phenol ring: A) phenols containing one, two or three hydroxy groups, and B) substituted phenols containing one hydroxy group in combination with halogen, nitro, methoxy and/or methyl substituents. Four different analyses were performed to determine the effects of the nature and the location of the substituent on biological activity. These include DPPH free radical scavenging activity, inhibition of ferroptosis, copper (II) ion reduction and copper-mediated DNA cleavage. Furthermore, molecular docking was used to probe structure-DNA affinity relationships.

2. RESULTS AND DISCUSSION

2.1. Design and synthesis of phenolic furanochromene hydrazones

Twenty-four phenolic furanochromene-hydrazones (**11a-11x**) were designed in order to determine structure-activity correlations. The compounds each have a phenol ring containing one, two or three hydroxy groups or a single hydroxy group, in combination with one or two additional substituents, including methoxy, methyl, nitro, bromo and/or iodo groups (Table 1). The target furanochromene hydrazone derivatives were synthesized in four steps using the reaction sequence outlined in Scheme 1. The first step of the reaction involves the formation of the dimethyl chromene (**7**) by the reaction of 2,4-dihydroxybenzaldehyde (**6**) and 3-methyl-2-butenal in the presence of triethylamine and calcium chloride dihydrate.[21] The furanochromene ester (**8**) was formed by reacting the chromene with methyl bromoacetate via the Rap-Stoermer reaction, which combines a nucleophilic substitution with an aldol-type reaction, followed by dehydration.[26,45]

Treatment of the furanochromene ester (**8**) with hydrazine hydrate gave the corresponding hydrazide (**9**). Condensation of the hydrazide with phenolic aldehydes (**10**) under reflux conditions

in the presence of catalytic acetic acid gave the phenolic furanochromene hydrazone derivatives **11a-11x** in 35-97% yield.

The successful formation of compounds **11a-11x** was confirmed by ^{1}H and ^{13}C NMR spectroscopy, which indicated that only one isomer was obtained for each compound. Further characterization was performed by IR and HRMS data. Notably, the imine hydrogen for the derivatives occurs between 8.19 ppm and 8.87 ppm in the ^{1}H NMR spectrum, influenced by the substituents on the phenol ring. The presence of the C=N bond was confirmed by stretching frequencies between 1630 and 1690 cm^{-1} in the IR spectrum.[48]

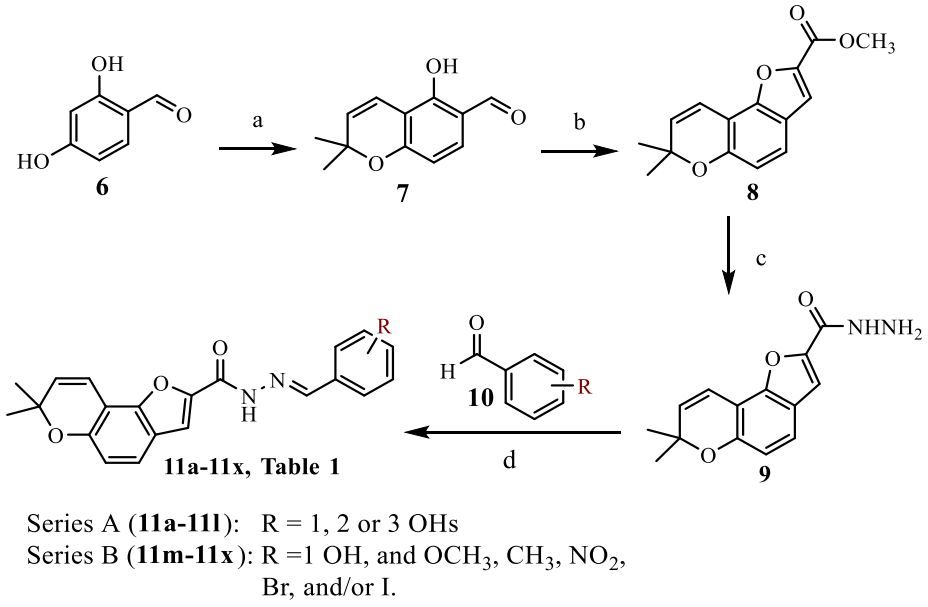

Series A (**11a-11l**): R = 1, 2 or 3 OHs
Series B (**11m-11x**): R =1 OH, and OCH_3, CH_3, NO_2, Br, and/or I.

Scheme 1. Synthesis of phenolic furanochromene hydrazone derivatives. *Reagents and conditions*. a) 3-methyl-2-butenal, Et_3N, $CaCl_2.2H_2O$, ethanol, reflux, 2h; b) methyl bromoacetate, K_2CO_3, DMF, rt for 1h, followed by gentle heating for 3 h; c) $NH_2NH_2{\cdot}H_2O$, ethanol, reflux, 2h; d) phenolic aldehyde, acetic acid, ethanol, reflux, 4-24 h.

Table 1. Structures, DPPH scavenging, and CUPRAC data for phenolic furanochromene hydrazone derivatives (**11a-11x**)

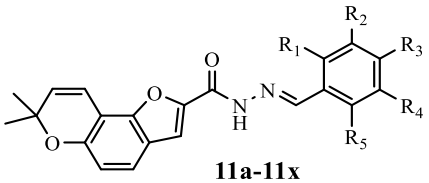

11a-11x

Compound	R_1	R_2	R_3	R_4	R_5	DPPH (IC_{50}, μM)	CUPRAC (TEAC)
11a	OH	OH	OH	H	H	10.11±0.45	2.89±0.04
11b	OH	H	OH	OH	H	24.33±0.60	2.43±0.04
11c	OH	H	OH	H	OH	81.05±4.73	1.36±0.03
11d	H	OH	OH	OH	H	27.85±0.37	2.59±0.06
11e	OH	OH	H	H	H	6.04±0.28	1.75±0.06
11f	OH	H	OH	H	H	70.14±1.2	1.42±0.03
11g	OH	H	H	OH	H	9.10±0.19	1.80±0.07
11h	H	OH	OH	H	H	5.92±0.14	3.97± 0.05
11i	H	OH	H	OH	H	>100	1.27±0.03
11j	OH	H	H	H	H	NA	0.48±0.09
11k	H	OH	H	H	H	NA	NDA
11l	H	H	OH	H	H	>100	0.79±0.02
11m	OH	OCH_3	H	H	H	>100	0.85±0.02
11n	OH	H	OCH_3	H	H	67.39±0.54	1.01±0.06
11o	OH	H	H	OCH_3	H	>100	1.22±0.04
11p	OH	H	H	CH_3	H	>100	0.95±0.07
11q	OH	H	OCH_3	H	OCH_3	>100	0.97±0.01
11r	H	OH	OCH_3	H	H	>100	1.36±0.02
11s	H	OCH_3	OH	H	H	87.79±6.10	1.75±0.06
11t	H	OCH_3	OH	OCH_3	H	ND	2.22±0.04
11u	H	CH_3	OH	CH_3	H	61.21±2.44	1.11±0.01
11v	H	OCH_3	OH	NO_2	H	> 00	1.52±0.01
11w	H	OCH_3	OH	Br	H	>100	1.09±0.04
11x	H	OCH_3	OH	I	H	>100	0.99±0.08
Ascorbic acid						51.18±0.25	0.72±0.06

Series A (**11a-11l**): mono, di and trihydroxylated phenols

Series B (**11m-11x**): substituted phenols containing one OH group

NA = No activity *ND = Not determined due to solubility problems*

2.2. Antioxidant evaluation

2.2.1. 2,2-Diphenyl-1-picrylhydrazyl (DPPH) free radical scavenging activity

Free radical scavenging ability of the phenolic furanochromene hydrazones **11a-11x** was determined using the in vitro DPPH assay. The DPPH radical is a nitrogen-centered radical that is stable at ambient temperature, and this method has been used widely to determine the free radical scavenging activities of phenolic compounds.[46-47,49-51] In this assay, the DPPH radical is reduced by an electron in the antioxidant, followed by protonation. The decrease in absorbance of a methanol solution of DPPH radical and antioxidant at 515 nm gives an indication of the free radical scavenging ability of a compound. IC_{50} data, where applicable, for the phenolic furanochromene hydrazone derivatives are shown in Table 1.

It is well documented that the number and location of hydroxy groups on the aromatic ring influences the DPPH free radical scavenging activity. However, there is less data comparing the effects of non-hydroxy substituent on the DPPH scavenging activity of compounds containing one hydroxy group on the phenol ring. Here, we compare the influence of number and location of hydroxy groups for series A compounds (**11a-11l**) and the influence of various substituents on the activity of monophenols for series B compounds (**11m-11x**). Among the trihydroxylated derivatives, the order of free-radical activity is **11a** > **11b** > **11d** > **11c**, with **11a** having an IC_{50} value of 10.11 μM and **11c** having an IC_{50} value of 81.05 μM. Based on this trend, it can be concluded that having the hydroxy groups contiguous to each other is favored. Among the dihydroxylated derivatives, **11e** and **11h**, with an *ortho*-dihydroxy pattern showed the best free radical scavenging activity (IC_{50} = 6.04 μM and 5.92 μM, respectively) among all of the compounds evaluated, including ascorbic acid (IC_{50} = 51.18 μM). Increased free radical scavenging activity for compounds having an *ortho*-dihydroxy pattern has previously been

reported, and can be rationalized based on the formation of a stable *ortho*-quinone after electron transfer.[50-51] The 2,5-dihydroxy derivative (**11g**) was comparable to **11a**, the 2,3,4-trihydroxy derivative. However, the 2,4-dihydroxy (**11f**) and 3,5-dihydroxy (**11i**) derivatives were significantly less effective, with IC_{50} values of 70.14 μM and greater than 100 μM, respectively.

It is expected that the compounds with only one hydroxy group would have lower free radical scavenging activity than those containing two or three. However, additional substituents such as methoxy, methyl, nitro or a halogen may exert additional effects on the free radical scavenging activity, depending on their location on the phenol ring. No detectable activity was observed for the 2-hydroxy derivative **11j,** and addition of methoxy groups to either position 3 (**11m**) or position 5 (**11o**) had no significant effect (IC_{50} > 100 μM). Similarly, addition of a methyl group at position 5 (**11p**) had no appreciable effect. By contrast, the addition of a methoxy group at position 4 (**11n**) led to increased activity (IC_{50} = 67.39 μM). Similar to the pattern observed between **11c** and **11f**, addition of a second methoxy group at position 6 (**11q**) led to a reduction in radical scavenging activity (IC_{50} > 100 μM), compared to **11n**.

The 3-hydroxy derivative (**11k**) also showed no detectable activity in the assay, while addition of an adjacent methoxy group at position 4 (**11r**), showed very slight improvement in activity (IC_{50} > 100 μM). The 4-hydroxy derivative (**11l**) also showed slight free radical scavenging activity (IC_{50} > 100 μM) compared to the 2-hydroxy and 3-hydroxy derivatives. There was marginal improvement in activity (IC_{50} = 87.79 μM) with the addition of an adjacent methoxy group at position 3 (**11s**), following the pattern observed for the other isomers containing adjacent hydroxy and methoxy groups.[49] While it would be expected that the addition of a second *ortho*-methoxy group at position 5 (**11t**) would further enhance activity, this was not verified due to the low solubility of the derivative in methanol and acetonitrile, which was used

as a substitute for methanol. Derivative **11u**, the corresponding dimethyl derivative of **11t** showed marginal activity (IC_{50} = 61.21 μM). Finally, the addition of a nitro, bromo or iodo group (**11v-11x**) ortho to the hydroxy group in **11s** led to a decline in activity (IC_{50} > 100 μM).

2.2.2. CUPRAC antioxidant activity

The phenolic furanochromene hydrazone derivatives (**11a-11x**) were also evaluated for their antioxidant effects using the CUPric ion Reducing Antioxidant Capacity (CUPRAC) method.[52] Although this is a robust method for determining antioxidant potential, it is underutilized. The CUPRAC method is based on the absorbance measurement of bis-neocuproine-Cu(I) chelate, formed as a result of the redox reaction of antioxidants with the CUPRAC reagent, bis(neocuproine)-Cu(II). The bis-neocuproine-Cu(II) chelate is blue-green in color. Upon the addition of the phenolic furanochromene hydrazones, a yellow-orange color develops as a result of the formation of the bis-neocuproine-Cu(I) charge-transfer complex, which absorbs at 450 nm. Increased absorbance at 450 nm indicates increased antioxidant activity.

Table 1 shows the Trolox Equivalent Antioxidant Capacity (TEAC) coefficients for the derivatives and ascorbic acid. The majority of the derivatives were more effective at reducing copper (II) ion than ascorbic acid, which gave a TEAC coefficient of 0.72. Among the series A compounds (**11a-11l**), compounds **11a, 11b, 11d** and **11h** had the highest activity, with TEAC values of 2.89, 2.43, 2.59 and 3.97, respectively. These four compounds have two or three OH groups on contiguous carbons, with one hydroxy group in a para position. The data indicate that these structural features play a role in the reducing capacity.[53] The 3,4-dihydroxy derivative (**11h**) had the best Cu (II) ion reducing capacity of all the derivatives. Notably, this compound

also had the highest free radical scavenging activity in the DPPH assay. Derivative **11e** has two contiguous hydroxy groups, and showed similar activity to **11h** in the DPPH scavenging assay. However, the lower TEAC score of 1.75 for **11e** in the CUPRAC assay may be due to interactions with copper due to the proximity of the *ortho*-hydroxy group with the adjacent imine nitrogen. The 3-hydroxy derivative (**11k**) did not show any detectable activity, while the 2-hydroxy and 4-hydroxy derivatives (**11j** and **11l**) showed lower reducing capacity than Trolox.

For the series B compounds (**11m-11x)**, derivative **11t** containing a para hydroxy group flanked by two methoxy groups on adjacent carbons was the most effective, with a TEAC coefficient of 2.22. Substitution of the two methoxy groups with methyl groups, **11u**, led to a significant decrease in activity, giving a TEAC coefficient of 1.11. This outcome can be rationalized based on the weaker electron donating ability of the methyl groups. Similarly, replacing one of the methoxy groups on **11t** with a different substituent reduces the activity. The nitro (**11v**), bromo (**11w**), and iodo (**11x**) derivatives gave TEAC scores of 1.52, 1.09 and 0.99, respectively. As expected, replacing one of the methoxy groups with a hydrogen atom, **11s**, also led to a significant reduction in activity to a TEAC coefficient of 1.75, which is identical to that observed for compound **11e**. Further reduction in activity was observed for the other four isomers of **11s**, with TEAC scores ranging from 0.85 for **11m** to 1.36 for **11r**. This outcome indicates that the hydroxy group is preferred in the para position, which is consistent with the data obtained for the series A compounds. As predicted based on electronic factors, **11p** is less active than **11o**. Similarly, **11q** was predicted and confirmed to be less active than its isomer **11t** due to the positioning of the methoxy groups relative to the OH group.

2.3. Inhibition of ferroptosis assays

Ferroptosis is a form of regulated cell death caused by iron-dependent lipid peroxidation. Ferroptosis is implicated in a number of neurodegenerative diseases and cancer. Since ferroptosis was discovered in 2012, several inhibitors have been developed. Phenolic compounds, possessing both iron chelation and anti-lipid peroxidation properties, have emerged as a class of potent inhibitors of ferroptosis.[34-35,54-57] Owing to its role as a potent ferroptosis inducer, erastin has been used in several cell lines to study ferroptosis induction or inhibition. In this study, erastin was used to develop a ferroptosis model in human keratinocytes (HaCaT) at a concentration of 20 μM. Phenolic furanochromene hydrazone derivatives **11a-11x** (5 μM) were evaluated for their cytoprotective potential by determining their ability to reverse erastin-induced ferroptosis (Fig. 2). Erastin decreased the cell viability of HaCaT cells to 45% as compared to the control group. More than half of the derivatives showed cytoprotective effects against erastin-induced ferroptosis by restoring the cell viability of HaCaT cells to 50% or above, and some distinct structure-activity relationships were observed.

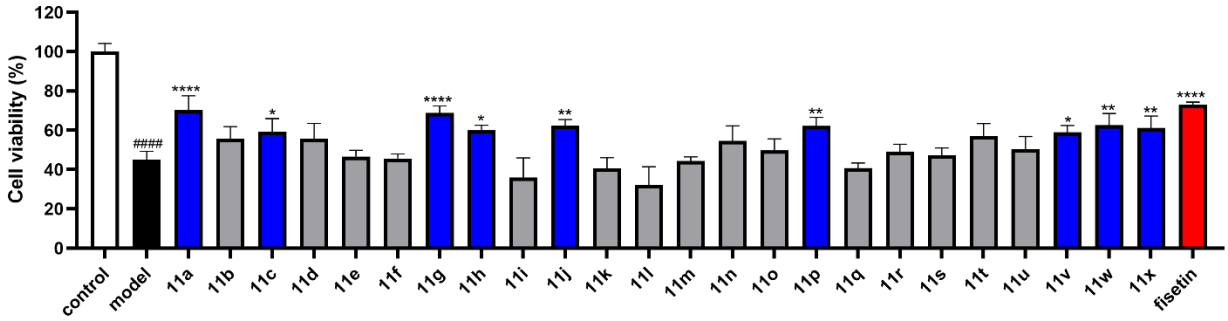

Fig. 2. Effects of the phenolic furanochromene hydrazone derivatives on erastin-induced ferroptosis in human keratinocyte HaCaT cells. Cells were incubated with test compounds (at 5 μM) for 4 h and then insulted with erastin (20 μM) for 24 h. The cell viability was then determined using the MTT assay. ####$p < 0.0001$ as compared to the control group; *$p < 0.05$, **$p < 0.01$, and ****$p < 0.0001$ as compared with model group. Compounds in blue bars show significant protective effects against erastin-induced ferroptosis in HaCaT cells.

Among the trihydroxylated derivatives (**11a-11d**), **11a** exhibited the greatest cytoprotective effect by restoring cell viability to 70%, and showed the best activity among all the derivatives. Derivatives **11b-11d** showed similar activity with 56-59% cell viability. Epigallocatechin gallate (EGCG) which contains pyrogallol groups has been shown to be an effective ferroptosis inhibitor.[57] Comparing derivatives **11a** and **11d** suggests that the proximity of the pyrogallol group to the imine group seems to enhance the inhibitory activity. Among the dihydroxy derivatives **11e-11i**, only **11g** and **11h** were effective at inhibiting ferroptosis; compounds **11e** and **11f** had little to no effect, while **11i** appears to enhance ferroptosis relative to erastin. Flavonoids and other compounds containing a catechol moiety, for example quercetin, butein, butin and carnosic acid, have demonstrated strong ferroptosis inhibition,[54-56] owing to their iron chelation properties and inhibition of lipid peroxidation by radical scavenging to generate stable quinones. With this in mind, the high inhibition of **11g** (69%) is not surprising as it could result in the formation of a para-quinone. By contrast, the ineffectiveness of **11e** was not predicted. The 2-hydroxy derivative **11j** was an effective ferroptosis inhibitor, while the isomeric 3-hydroxy and 4-hydroxy derivatives (**11k** and **11l**) enhanced ferroptosis induction. Among the isomeric methoxy phenols **11m-11o** and **11r-11s**, only **11n** showed cell viability above 50%, with the others showing viability between 44 and 50%. The influence of location of methoxy groups is also evident in comparing **11q** (41%) and **11t** (57%). This can perhaps be rationalized based on differences in radical scavenging activity, where a radical generated by **11t** can be stabilized by the adjacent methoxy groups. Further structure activity correlations are revealed by substituting methoxy groups with methyl groups. For **11p**, this substitution enhances inhibition relative to **11o**. Conversely, the cell viability is diminished for **11u** relative to **11t**. Finally,

replacing one of the methoxy groups in **11t** with nitro, bromo, and iodo groups slightly enhanced cell protection, with the bromo substitution being most effective.

2.4. DNA cleavage studies

All of the phenolic furanochromene hydrazone derivatives were evaluated for plasmid pBR322 DNA cleavage in the absence of copper (II) ion and showed no activity. Upon incubation with copper (II) acetate at 37°C for 24 hours, most derivatives (1 mM) showed DNA cleavage to open-circular (OC, one strand breakage) and/or linear (two strand breakage) forms, with a few also having the uncleaved supercoiled (SC) DNA present. Fig. 3 shows the DNA cleavage profile for the series A derivatives (**11a-11l**). Derivatives **11b** and **11h** showed no evidence of DNA on the gel, indicating cleavage of DNA to smaller fragments which ran off the gel during electrophoresis. Both compounds have a hydroxy group at position 4, with a second hydroxy group adjacent, and showed strong copper (II) ion reducing activity in the CUPRAC assay. This observation is consistent with that observed for flavonoids containing the *ortho*-dihydroxy pattern.[58-59] Derivatives **11a, 11g** and **11i-11l**, showed predominantly the open-circular form of DNA with little or no linear or supercoiled forms. While derivatives **11c-11e** showed cleaved forms of DNA, there was also a significant amount of the supercoiled form. Derivative **11f** was comparable to the DNA control, showing mostly supercoiled DNA.

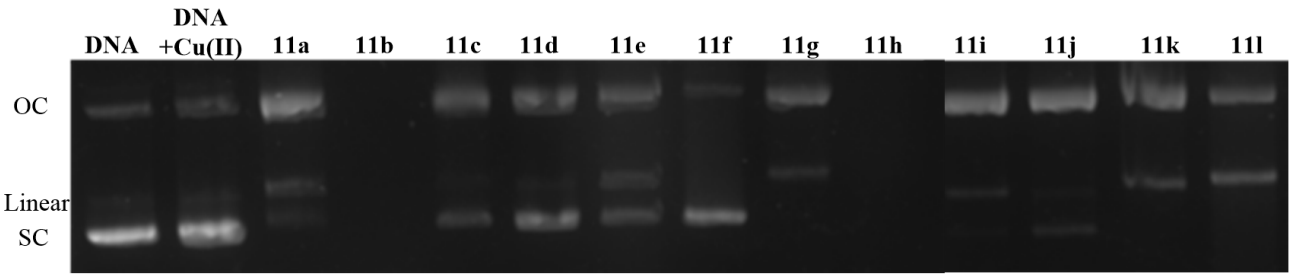

Fig. 3. Agarose gel electrophoretic pattern of pBR322 plasmid DNA after treatment with

compounds **11a-11l** in the presence of copper (II) acetate. *Lane 1:* DNA control; *Lane 2:* DNA + $Cu(OAc)_2$; *Lanes 3-14:* DNA + $Cu(OAc)_2$ + test compounds as indicated.

The electrophoresis pattern for the series B derivatives (**11m-11x**) are displayed in Fig. 4. Derivatives containing a hydroxy group in the ortho position (**11m-11q**) clearly showed all three forms of DNA, with the open-circular form predominant. Derivatives containing a hydroxy group in the meta or para position (**11r-11x**) also showed predominantly the open-circular form, with small amounts of the linear form. However, there is little or no evidence of the supercoiled form, indicating that they were more effective at cleaving plasmid DNA than the ortho-hydroxy compounds. While there was some correlation between the copper (II) ion reducing capacity and DNA cleavage ability for the derivatives, this pattern was not consistent for all of the derivatives.

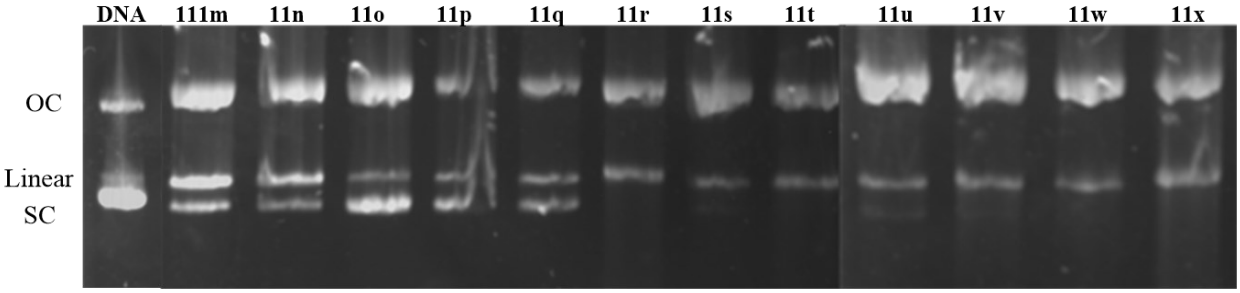

Fig. 4. Agarose gel electrophoretic pattern of pBR322 plasmid DNA after treatment with compounds **11m-11x** in the presence of copper (II) acetate. *Lane 1:* DNA control; *Lanes 2-13:* DNA + $Cu(OAc)_2$ + test compounds as indicated.

Owing to its strong copper (II) ion reducing and copper-mediated DNA cleaving capacity, compound **11h** was evaluated for concentration dependent cleavage using a concentration range of 3.9 to 500 μM. At the higher concentrations, there was evidence of linear and/or open circular forms of DNA, together with some fragmentation as evidenced by streaking (Supplementary data, Fig. S81). At the lowest concentration there was evidence of both linear

and open circular forms, but no evidence of the supercoiled form, indicating that compound **11h** is a very effective DNA cleavage agent. Although not evaluated for concentration dependence, some of the other derivatives are likely to show DNA cleavage at the lower concentrations.

2.5. DNA molecular docking studies

Molecular docking is a useful tool to gain understanding of the noncovalent interactions between drug molecules and their targets. Here, the phenolic furanochromene hydrazone derivatives (**11a-11x**) were analyzed to determine their binding affinity to the DNA duplex sequence d(CGCGAATTCGCG)$_2$ (PDB: 1BNA). As indicated by Neidle,[60] this Dickerson-Drew dodecamer approximates closely to the original Watson-Crick model for B-DNA, and therefore is useful for studying interactions of small molecules with DNA. The phenolic furanochromene hydrazone derivatives interacted with both strands of DNA and showed a preference for minor groove binding in G-C rich regions. Binding affinities for the lowest energy conformations of the derivatives ranged from -9.5 to -10.9 kcal/mol (Table 1). These values are comparable to that of the anticancer drug ibrutinib, with a reported docking score of -10.4 kcal/mol using the same DNA sequence.[61] The derivatives showed two modes of binding. Compounds **11a-11g** had the chromene moiety embedded in the interior of the helix (Fig. 5A), while the phenolic portion was embedded towards the end of the helix. Compounds **11h-11x** had the two portions of the molecules oriented in the opposite direction (Fig. 5B). Except for compounds **11j**, **11n** and **11p**, all compounds showed hydrogen bonding interaction between the carbonyl carbon on the furanochromene derivative and guanine residues at positions 10 and 16. Compounds **11j**, **11n** and **11p** are stabilized by interactions between the furan oxygen atom and guanine residue 16 (Supplementary data, Fig. S82 and Fig. S83).

Table 2. DNA docking data for phenolic furanochromene hydrazone derivatives (**11a-11x**) compared to Ibrutinib

Compound	DNA docking (kcal/mol)	Compound	DNA docking (kcal/mol)
11a	-10.8	**11m**	-10.2
11b	-10.4	**11n**	-9.6
11c	-10.6	**11o**	-9.7
11d	-9.8	**11p**	-9.8
11e	-10.9	**11q**	-9.8
11f	-10.5	**11r**	-9.6
11g	-10.5	**11s**	-9.8
11h	-9.9	**11t**	-9.7
11i	-9.5	**11u**	-9.8
11j	-9.7	**11v**	-9.9
11k	-9.6	**11w**	-10.0
11l	-9.8	**11x**	-9.9
Ibrutinib	-8.7		

Trihydroxy and dihydroxy derivatives (**11a-c** and **11e-g**), incorporating a hydroxy group *ortho* to the imine group showed the best binding affinities (-10.4 to -10.9 kcal/mole). The binding interactions for this group of compounds is exemplified by derivative **11a** (Fig. 5C). The DNA-furanochromene hydrazone complex is stabilized by hydrogen bonding interactions between the *ortho* hydroxy group and the oxygen atom of the cytosine residue at position 11, and between the oxygen atom of *meta* hydroxy group and a hydrogen atom in the guanine residue at position 14. Further stabilization is achieved through hydrogen bonding between the hydrazone hydrogen and the oxygen atom of the ribose residue at position 17. The lower docking affinity for derivative **11d** can be attributed to the loss of interaction to cytosine residue at position 11 due to the lack of an *ortho* hydroxy group. The docking affinities for compounds **11h-11x** ranged from -9.5 to -10.2 kcal/mol. The interactions for compound **11w** with a docking score of -10.2 kcal/mol are shown in Fig. 5D. In addition to the hydrogen bonding interactions previously described for the carbonyl carbon, the hydrogen on the *para*-hydroxy group interacts with an

oxygen atom from the phosphate group at position 10. 2D-interaction maps for all derivatives are shown in Fig. S82 and Fig. S83 (Supplementary data).

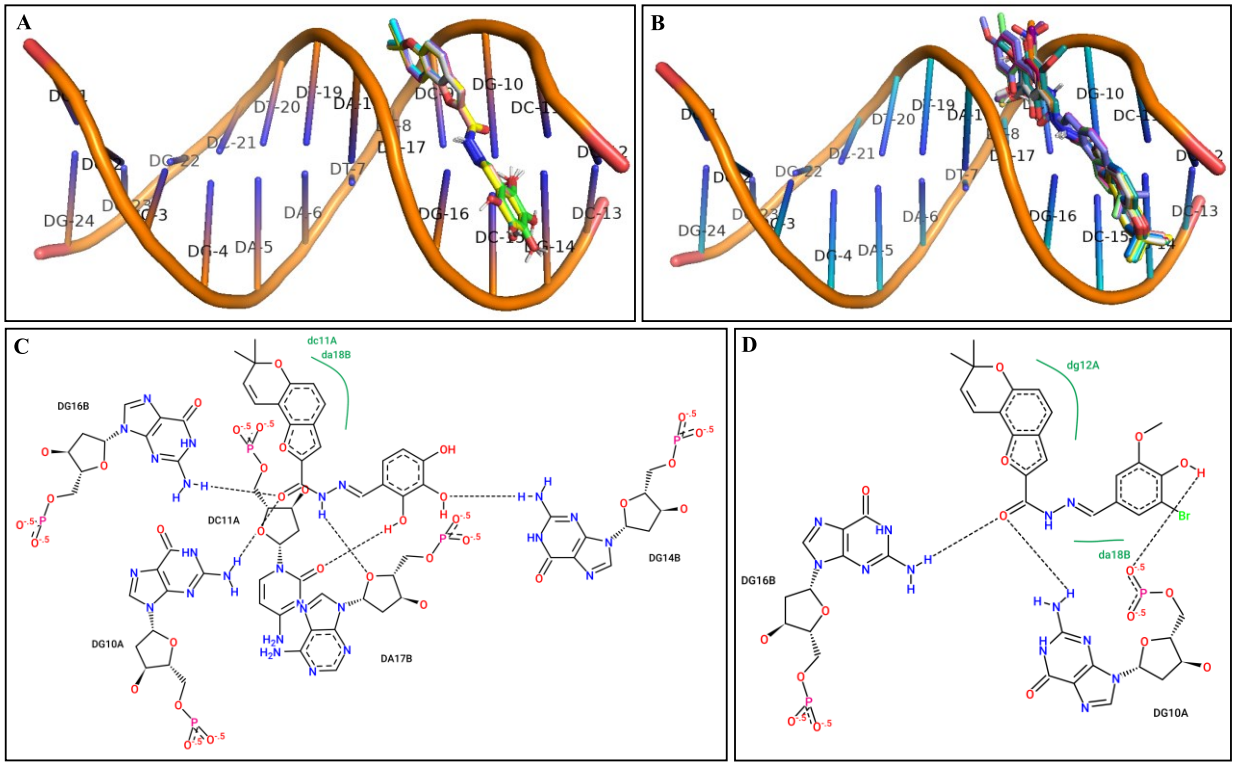

Fig. 5. Interaction of phenolic furanochromene hydrazones with DNA (PDB ID: 1BNA): Chain A: CGCGAATTCGCG (1-12); Complementary Chain B: GCGCTTAAGCGC (13-24). A) Pymol 3D View of DNA with **11a-11g**; (B) Pymol 3D View of DNA with **11h-11x**; (C) PoseView interaction diagram for DNA with **11a**; (D) PoseView interaction diagram for DNA with **11w**.

3. CONCLUSIONS

In conclusion, a series of phenolic furanochromene hydrazone derivatives with varying substituents on the phenol ring were synthesized and evaluated for free radical scavenging, copper (II) ion reducing, ferroptosis inhibiting and DNA cleavage properties. Compounds containing *ortho*-dihydroxy or *para*-dihydroxy substitution patterns were most effective as free radical scavengers and copper (II) ion reducers. Most of the compounds reversed erastin-induced

ferroptosis in HaCaT cells, indicating their cytoprotective potential. In addition, all but one of the compounds showed copper-mediated cleavage of plasmid DNA. Interactions with DNA were confirmed by molecular docking studies, which showed that all compounds were minor grove binders with preference for binding to GC rich areas. These data indicate that the phenolic furanochromene hydrazone derivatives are effective antioxidant agents and also have the potential to serve as anticancer agents due to their strong interaction with DNA.

4. MATERIALS AND METHODS

4.1. Instruments and reagents

All chemicals and solvents were purchased from Sigma Aldrich, Fisher Scientific or TCI America. Reactions were monitored by TLC on silica gel plates obtained from Sigma-Aldrich. Column chromatography was carried out on a Teledyne CombiFlash Rf 200, using RediSep Gold silica gel columns, and eluting with ethyl acetate-hexane solvent gradients. Melting points were recorded on RD-MP or Thomas Hoover capillary melting point instruments and values are uncorrected. FTIR spectra were recorded on a Nicolet iS50 spectrometer, equipped with attenuated total reflectance (ATR) apparatus. NMR data (^{1}H, 400 MHz and ^{13}C, 100 MHz) were recorded on a JEOL 400 MHz instrument (NSF MRI: CHE-1625340) using $CDCl_3$ and DMSO-d_6 as solvents. High resolution mass spectrometry data were acquired on an Agilent 6560 ion mobility Q-ToF mass spectrometer with Agilent Jet Spray dual ESI inlet (NSF MRI: CHE-2018547). Samples were run in positive mode by flow injection analysis in LC-MS grade 50% acetonitrile and 50% water containing 0.1% formic acid. The CUPRAC assay was carried out with a Carey UV-Vis spectrometer, and DPPH assays were conducted using a SpectraMax

microplate reader (Molecular Devices). DNA gels were read with a Western Blot imager (Azure Biosystems).

4.2. Synthesis

4.2.1. Synthesis of chromene 7 (5-hydroxy-2,2-dimethyl-2H-chromene-6-carbaldehyde)

Calcium chloride dihydrate (6.34 g, 43.1 mmol) and triethylamine (24.0 mL, 172.2 mmol) were added to a solution of 2,4-dihydroxy benzaldehyde (7.15 g, 51.8 mmol) and 3-methyl-2-butenal (10.3 mL, 107.5 mmol) in absolute ethanol (175 mL), and the reaction mixture was heated under reflux for 1.5 hours. After cooling, the mixture was cooled to room temperature, acidified with 25 % HCl, and the ethanol was removed in vacuo. The resulting mixture was diluted with distilled water (50 mL), and extracted with ethyl acetate (4 × 50 mL). The combined organic extract was dried over anhydrous sodium sulfate, filtered, and concentrated *in vacuo*. Silica gel column chromatography of the residue using 5% ethyl acetate-hexanes afforded chromene **7** as an amorphous yellow solid (6.47 g, 61 %).

M.p.: 68-70 ˚C, lit 69-70 °C;[26,62] IR (ATR), cm^{-1}: 1655, 1624, 1578, 1467. ^{1}H NMR ($CDCl_3$) δ: 11.63 (1H, s), 9.64 (s, 1H), 7.27 (d, J = 8.4 Hz, 1H), 6.67 (d, J = 10.0 Hz, 1H), 6.40 (d, J = 8.4 Hz, 1H), 5.59 (d, J = 10.0 Hz, 1H), 1.45 (s, 6H). ^{13}C NMR ($CDCl_3$) δ: 194.4, 160.4, 158.5, 134.6, 128.4, 115.2, 115.1, 109.3, 108.7, 78.0, 28.3.

HRMS (ESI): m/z 205.0869 [M + H] +; calcd. for $C_{12}H_{12}O_3$, 205.0859.

4.2.2. Synthesis of furanochromene 8 (Ethyl 7,7-dimethyl-7H-furo[2,3-f]chromene-2-carboxylate)

Methyl bromoacetate (4 mL, 43.4 mmol) was added dropwise to a suspension of chromene **7** (4.53 g, 22.2 mmol) and potassium carbonate (12.21 g, 88.3 mmol) in anhydrous dimethylformamide (80 mL). The mixture was stirred at room temperature for 1 h, followed by gentle heating for 3 hours. The reaction mixture was cooled and diluted with water (150 mL), followed by extraction with ethyl acetate (3 × 50 mL). The combined organic layer was dried over sodium sulfate, filtered and concentrated *in vacuo*. The residue was purified by column chromatography using 5% ethyl acetate-hexanes to give furanochromene **8** as an off-white solid (2.46 g, 43%).

M.p.: 78-80 ˚C; IR (ATR), cm^{-1}: 1731, 1638, 1567, 1482. ^{1}H NMR ($CDCl_3$) δ: 7.42 (s, 1H), 7.35 (d, 1H, *J* = 8.4 Hz), 6.87 (d, 1H, *J* = 10.0 Hz), 6.78 (d, 1H, *J* = 8.4 Hz), 5.68 (d, 1H, *J* = 10.0 Hz), 3.93 (s, 3H), 1.45 (s, 6H). ^{13}C NMR ($CDCl_3$) δ: 160.1, 153.2, 152.3, 144.8, 130.5, 122.1, 120.5, 115.7, 114.8, 114.6, 106.7, 77.0, 52.2, 27.9. HRMS (ESI): *m/z* 259.0864 [M + H] +; calcd. for $C_{15}H_{15}O_4$, 259.0926

4.2.3. Synthesis of furanochromene Hydrazide 9 (7,7-dimethyl-7H-furo[2,3-f]chromene-2-carbohydrazide)

A solution of furanochromene **8** (3.05 g, 11.8 mmol) and hydrazine hydrate monohydrate (1.25 mL, 25.8 mol) in absolute ethanol (12 mL) was heated under reflux for 3.5 h. The solvent was removed *in vacuo* to give an oil. Water (40 mL) was added and a precipitated was formed. The solid was filtered and recrystallized from water-ethanol to give the furanochromene hydrazide **9** as a pale yellow solid (2.73 g, 90%).

M.p.: 139-141 ˚C; IR (ATR), cm^{-1}: 3305, 3209, 1676, 1641, 1587, 1517.

^{1}H NMR (DMSO-d_6) δ: 9.89 (s, 1H, NH), 7.41 (d, 1H, *J* = 8.4 Hz), 7.36 (s, 1H), 6.81 (d, 1H, *J* = 10.0 Hz), 6.74 (d, 1H, *J* = 8.4 Hz), 5.86 (d, 1H, *J* = 10.0 Hz), 4.53 (s, 2H, NH_2), 1.38 (s, 6H). ^{13}C NMR (DMSO-d_6) δ: 158.5, 152.0, 150.8, 148.2, 131.8, 122.5, 121.1, 115.5, 114.0, 109.8, 106.4, 77.2, 27.9. HRMS (ESI): *m/z* 259.0404 [M + H] +; calcd. for $C_{14}H_{15}N_2O_3$, 259.1082

4.2.4. General synthesis of substituted furanochromene hydrazone derivatives

Acetic acid (50 μL) was added dropwise to a mixture of furanochromene hydrazide (250 mg, 0.96 mmol) and substituted benzaldehyde (0.96 mmol) in methanol (5 mL). The mixture was heated under reflux for 4 to 24 hours, with stirring, followed by the addition of water (20 mL). The mixture was filtered and the crude product was recrystallized with ethanol or ethanol-water mixtures to afford the corresponding hydrazones as white or yellow solids (35% to 97 %).

(E)-7,7-dimethyl-N'-(2,3,4-trihydroxybenzylidene)-7H-furo[2,3-f]chromene-2-carbohydrazide (11a)

Pale yellow solid. Yield: 97%. M.p.: 227-229 ˚C; IR (ATR), cm^{-1}: 3523, 3165, 1640, 1615, 1598, 1579, 1485, 1271, 1210, 1156, 1123, 1067, 714.

^{1}H NMR (DMSO-d_6) δ: 12.00 (s, 1H, OH), 11.26 (s, 1H, NH), 9.50 (s, 1H, OH), 8.51 (s, 1H, OH), 8.50 (s, 1H, CH=N), 7.58 (s, 1H), 7.48 (d, 1H, *J* = 8.4 Hz), 6.84 (d, 1H, *J* = 10.0 Hz), 6.79 (d, 1H, *J* = 8.4 Hz), 6.78 (d, 1H, *J* = 8.0 Hz), 6.38 (d, 1H, *J* = 8.0 Hz), 5.90 (d, 1H, *J* = 10.0 Hz), 1.40 (s, 6H). ^{13}C NMR (DMSO-d_6) δ: 154.6, 152.6, 151.1, 151.0, 149.5, 148.0, 147.5, 133.3, 131.9, 122.9, 121.6, 121.1, 115.4, 114.5, 111.9, 111.4, 108.3, 106.4, 77.4, 27.9.

HRMS (ESI): *m/z* 395.1261 [M + H] +; calcd. for $C_{21}H_{19}N_2O_6$, 395.1243

(E)-7,7-dimethyl-N'-(2,4,5-trihydroxybenzylidene)-7H-furo[2,3-f]chromene-2-carbohydrazide (11b)

Yellow solid. Yield: 84%. M.p.: >250˚C; IR (ATR), cm^{-1}: 3543, 3480, 3420, 3049, 1640, 1621, 1594, 1575, 1294, 1270, 1205, 1155, 1118, 1065, 704.

^{1}H NMR (DMSO-d_6) δ: 11.81 (s, 1H, NH), 10.32 (s, 1H, OH), 9.55 (s, 1H, OH), 8.60 (s, 1H, OH), 8.50 (s, 1H, CH=N), 7.55 (s, 1H), 7.48 (d, 1H, *J* = 8.4 Hz), 6.92 (s, 1H), 6.85 (d, 1H, *J* = 10.0 Hz), 6.79 (s, 1H, *J* = 8.4 Hz), 6.31 (s, 1H), 5.90 (d, 1H, *J* = 10.0 Hz), 1.41 (s, 6H). ^{13}C NMR (DMSO-d_6) δ: 154.6, 152.5, 152.4, 151.1, 150.1, 149.0, 147.7, 139.2, 131.9, 122.9, 121.1, 115.5, 114.6, 114.4, 111.6, 110.1, 106.4, 104.0, 77.4, 27.9.

HRMS (ESI): *m/z* 395.1255 [M + H] +; calcd. for $C_{21}H_{19}N_2O_6$, 395.1243

(E)-7,7-dimethyl-N'-(2,4,6-trihydroxybenzylidene)-7H-furo[2,3-f]chromene-2-carbohydrazide (11c)

Red/brown solid. Yield: 85%. M.p.: >250 ˚C; IR (ATR), cm^{-1}: 3563, 3170, 1631, 1596, 1578, 1482, 1269, 1208, 1156, 1115, 1065, 701.

^{1}H NMR (DMSO-d_6) δ: 11.96 (s, 1H, NH), 11.04 (s, 1H, OH), 9.85 (s, 1H, OH), 8.83 (s, 1H, CH=N), 7.55 (s, 1H), 7.48 (d, 1H, *J* = 8.4 Hz), 6.85 (d, 1H, *J* = 10.0 Hz), 6.79 (d, 1H, *J* = 8.4 Hz), 5.90 (d, 1H, *J* = 10.0 Hz), 5.82 (s, 1H), 1.41 (s, 6H). ^{13}C NMR (DMSO-d_6) δ: 162.3, 160.3, 154.3, 152.5, 151.1, 147.8, 147.5, 131.9, 122.9, 121.1, 115.5, 114.4, 111.8, 106.4, 99.6, 94.9, 77.4, 27.9.

HRMS (ESI): *m/z* 395.1263 [M + H] +; calcd. for $C_{21}H_{19}N_2O_6$, 395.1243

(E)-7,7-dimethyl-N'-(3,4,5-trihydroxybenzylidene)-7H-furo[2,3-f]chromene-2-carbohydrazide (11d)

Pale yellow solid. Yield: 97%. M.p.: 245-246 ˚C. IR (ATR), cm^{-1}: 3342, 1641, 1616, 1595, 1524, 1327, 1306, 1268, 1203,1152, 1114, 1062, 1006, 725.

^{1}H NMR (DMSO-d_6) δ: 8.19 (s, 1H, CH=N), 7.54 (s, 1H), 7.47 (d, 1H, *J* = 8.4 Hz), 6.84 (d, 1H, *J* = 10.0 Hz), 6.79 (d, 1H, *J* = 8.4 Hz), 6.68 (s, 2H), 5.90 (d, 1H, *J* = 10.0 Hz), 1.40 (s, 6H). ^{13}C NMR (DMSO-d_6) δ: 154.8, 152.4, 151.0, 149.7, 147.9, 146.7, 136.5, 131.9, 124.9, 122.8, 121.1, 115.5, 114.4, 111.5, 106.9, 106.4, 77.4, 27.9.

HRMS (ESI): *m/z* 395.1253 [M + H] +; calcd. for $C_{21}H_{19}N_2O_6$, 395.1243

(E)-N'-(2,3-dihydroxybenzylidene)-7,7-dimethyl-7H-furo[2,3-f]chromene-2-carbohydrazide (11e)

Pale yellow solid. Yield: 77%. M.p.: >250 ˚C; IR (ATR), cm^{-1}: 3261, 1638, 1553, 1479, 1373, 1270, 1199, 1161, 1111, 1066, 723.

^{1}H NMR (DMSO-d_6) δ: 12.14 (s, 1H, NH), 10.83 (s, 1H, OH), 9.28 (d, 1H, OH), 8.65 (s, 1H, CH=N), 7.62 (s, 1H), 7.50 (s, 1H, *J* = 8.4 Hz), 6.98 (d, *J* = 7.6 Hz) 6.85 (d, 1H, *J* = 10.0 Hz), 6.84 (d, 1H, *J* = 7.6 Hz), 6.80 (*J* = 8.4 Hz), 6.72 (t, 1H, *J* = 7.6 Hz), 5.91 (d, 1H, *J* = 10.0 Hz), 1.41 (s, 6H). ^{13}C NMR (DMSO-d_6) δ: 154.9, 152.6, 151.2, 149.6, 147.3, 146.6, 146.2, 131.9, 123.0, 121.1, 120.2, 119.8, 119.5, 118.0, 115.4, 114.5, 112.2, 106.4, 77.4, 27.9.

HRMS (ESI): *m/z* 379.1314 [M + H] +; calcd. for $C_{21}H_{19}N_2O_5$, 379.1294

(E)-N'-(2,4-dihydroxybenzylidene)-7,7-dimethyl-7H-furo[2,3-f]chromene-2-carbohydrazide (11f)

Pale yellow solid. Yield: 52%. M.p.: >250 ˚C; IR (ATR), cm^{-1}: 3256, 3109, 1643,1627, 1592, 1458, 1360, 1333, 1264, 1233, 1155, 1111, 1060, 732.

^{1}H NMR (DMSO-d_6) δ: 11.95 (s, 1H, OH), 11.21 (s, 1H, NH), 9.97 (s, 1H, OH), 8.55 (s, 1H, CH=N), 7.57 (s, 1H), 7.48 (d, 1H, *J* = 8.4 Hz), 7.32 (d, 1H, *J* = 8.4 Hz), 6.85 (d, 1H, *J* = 10.0 Hz), 6.80 (d, 1H, *J* = 8.4 Hz), 6.34 (d, 1H, *J* = 8.4 Hz), 6.30 (s, 1H), 5.90 (d, 1H, *J* = 10.0 Hz), 1.40 (s, 6H). ^{13}C NMR (DMSO-d_6) δ: 161.4, 159.9, 154.7, 152.5, 151.1, 149.8, 147.5, 131.9, 131.5, 122.9, 121.1, 115.4, 114.5, 111.8, 111.2, 108.4, 106.4, 103.2, 77.4, 27.9.

HRMS (ESI): *m/z* 379.1305 [M + H] +; calcd. for $C_{21}H_{19}N_2O_5$, 379.1294

(E)-N'-(2,5-dihydroxybenzylidene)-7,7-dimethyl-7H-furo[2,3-f]chromene-2-carbohydrazide (11g)

Yellow solid. Yield: 90%. M.p.: 240-243 ˚C; IR (ATR), cm^{-1}: 3545, 3204, 1644, 1621, 1592, 1578, 1484, 1376, 1272, 1207, 1158, 1113, 1066, 725.

^{1}H NMR (DMSO-d_6) δ: 12.00 (s, 1H, NH), 10.13 (s, 1H, OH), 8.97 (d, 1H, OH), 8.62 (s, 1H, CH=N), 7.60 (s, 1H), 7.49 (d, 1H, *J* = 8.4 Hz), 7.01 (s, 1H), 6.85 (d, 1H, *J* = 10.0 Hz), 6.80 (d, 1H, *J* = 8.4 Hz), 6.73 (d, 1H, *J* = 8.8 Hz), 6.71 (d, 1H, *J* = 8.8 Hz), 5.90 (d, 1H, *J* = 10.0 Hz), 1.40 (s, 6H). ^{13}C NMR (DMSO-d_6) δ: 154.9, 152.6, 151.1, 150.7, 150.5, 148.0, 147.5, 131.9, 123.0, 121.1, 119.8, 119.7, 117.6, 115.5, 114.5, 113.7, 112.0, 106.4, 77.4, 27.9.

HRMS (ESI): *m/z* 379.1199 [M + H] +; calcd. for $C_{21}H_{19}N_2O_5$, 379.1294

(E)-N'-(3,4-dihydroxybenzylidene)-7,7-dimethyl-7H-furo[2,3-f]chromene-2-carbohydrazide (11h)

Pale yellow solid. Yield: 72%. M.p.: 151-153 ˚C; IR (ATR), cm^{-1}: 3218, 1640, 1591, 1516, 1483, 1268, 1200, 1156, 1112, 1062, 728.

^{1}H NMR (DMSO-d_6) δ: 11.65 (s, 1H, NH), 9.42 (s, 1H, OH), 9.29 (s, 1H, OH), 8.28 (s, 1H, CH=N), 7.55 (s, 1H), 7.47 (d, 1H, *J* = 8.4 Hz), 7.23 (s, 1H), 6.92 (d, 1H, *J* = 7.6 Hz), 6.85 (d, 1H, *J* = 10.0 Hz), 6.78 (d, 1H, *J* = 8.4 Hz), 6.76 (d, 1H, *J* = 7.6 Hz), 5.89 (d, 1H, *J* = 10.0 Hz), 1.40 (s, 6H). ^{13}C NMR (DMSO-d_6) δ: 154.9, 152.4, 151.0, 149.4, 148.7, 147.9, 146.3, 131.9, 126.1, 122.8, 121.3, 121.1, 116.1, 115.5, 114.4, 113.2, 111.5, 106.4, 77.4, 27.9.

HRMS (ESI): *m/z* 379.1306 [M + H] +; calcd. for $C_{21}H_{19}N_2O_5$, 379.1294

(E)-N'-(3,5-dihydroxybenzylidene)-7,7-dimethyl-7H-furo[2,3-f]chromene-2-carbohydrazide (11i)

Pale yellow solid. Yield: 86%. M.p.: >250 ˚C; IR (ATR), cm^{-1}: 3335, 3226, 1665, 1640, 1578, 1486, 1340, 1303, 1259, 1205, 1160, 1111, 1065, 1005, 728.

^{1}H NMR (DMSO-d_6) δ: 11.77 (s, 1H, NH), 9.46 (s, 2H, OH), 8.27 (s, 1H, CH=N), 7.58 (s, 1H), 7.49 (d, 1H *J* = 8.4 Hz), 6.86 (d, 1H, *J* = 10.0 Hz), 6.80 (s, 1H, *J* = 8.4 Hz), 6.59 (s, 2H), 6.25 (s, 1H), 5.90 (d, 1H, *J* = 10.0 Hz), 1.41 (s, 6H). ^{13}C NMR (DMSO-d_6) δ: 159.3, 155.1, 152.6, 151.1, 149.2, 147.7, 136.3, 131.9, 122.9, 121.1, 115.5, 114.5, 111.9, 106.4, 105.8, 105.2, 77.4, 27.9.

HRMS (ESI): *m/z* 379.1297 [M + H] +; calcd. for $C_{21}H_{19}N_2O_5$, 379.1294

(E)-N'-(2-hydroxybenzylidene)-7,7-dimethyl-7H-furo[2,3-f]chromene-2-carbohydrazide (11j)

Pale yellow solid. Yield: 65%. M.p.: 238-239 ˚C; IR (ATR), cm^{-1}: 3228, 1652, 1622, 1610, 1584, 1526, 1484, 1366, 1298, 1263, 1195, 1157, 1109, 1068, 733.

^{1}H NMR (DMSO-d_6) δ: 12.12 (s, 1H, NH), 11.03 (s, 1H, OH), 8.70 (s, 1H, CH=N), 7.62 (s, 1H), 7.57 (d, 1H, d, *J* = 7.2 Hz), 7.50 (s, 1H, d, *J* = 8.4 Hz), 7.28 (t, 1H, *J* = 7.2 Hz), 6.92 (d, 1H, *J* = 7.2 Hz), 6.90 (t, 1H, *J* = 7.2 Hz), 6.85 (d, 1H, *J* = 10.0 Hz), 6.80 (d, 1H, *J* = 8.4 Hz), 5.90 (d, 1H, *J* = 10.0 Hz), 1.41 (s, 6H). ^{13}C NMR (DMSO-d_6) δ: 157.9, 155.0, 152.6, 151.2, 148.8, 147.4, 132.1, 131.9, 129.6, 123.0, 121.1, 120.0, 119.4, 116.9, 115.4, 114.5, 112.2, 106.4, 77.4, 27.9.

HRMS (ESI): *m/z* 363.1361 [M + H] +; calcd. for $C_{21}H_{19}N_2O_4$, 363.1345

(E)-N'-(3-hydroxybenzylidene)-7,7-dimethyl-7H-furo[2,3-f]chromene-2-carbohydrazide (11k)

Pale yellow solid. Yield: 91%. M.p.: 213-214 ˚C; IR (ATR), cm^{-1}: 3551, 3190, 1640, 1614, 1581, 1455, 1371, 1305, 1272, 1206, 1155, 1113, 1062, 725.

^{1}H NMR (DMSO-d_6) δ: 11.84 (s, 1H, NH), 9.64 (s, 1H, OH), 8.39 (s, 1H, CH=N), 7.60 (s, 1H), 7.49 (d, 1H, *J* = 8.4 Hz), 7.26-7.20 (m, 2H), 7.09 (d, 1H, *J* = 7.2 Hz), 6.89-6.79 (m, 3H), 5.90 (d, 1H, *J* = 10.0 Hz), 1.41 (s, 6H). ^{13}C NMR (DMSO-d_6) δ: 158.3, 155.1, 152.6, 151.1, 149.0, 147.7, 135.9, 131.9, 130.5, 122.9, 121.1, 119.5, 118.2, 115.5, 114.5, 113.2, 111.9, 106.4, 77.4, 27.9.

HRMS (ESI): *m/z* 363.1359 [M + H] +; calcd. for $C_{21}H_{19}N_2O_4$, 363.1345

(E)-N'-(4-hydroxybenzylidene)-7,7-dimethyl-7H-furo[2,3-f]chromene-2-carbohydrazide (11l)

Pale yellow solid. Yield: 55%. M.p.: 237-238 ˚C; IR (ATR), cm^{-1}: 3218, 1641, 1601, 1588, 1512 1267, 1200, 1113, 1062, 729.

^{1}H NMR (DMSO-d_6) δ: 11.69 (s, 1H, NH), 9.94 (s, 1H, OH), 8.37 (s, 1H, CH=N), 7.56 (s, 1H), 7.55 (d, 2H, *J* = 8.4 Hz), 7.47 (d, 1H, *J* = 8.4 Hz), 6.85 (d, 1H, *J* = 10.0 Hz), 6.82 (d, 2H, *J* = 8.4 Hz), 6.78 (d, 1H, *J* = 8.4 Hz), 5.89 (d, 1H, *J* = 10.0 Hz), 1.39 (s, 6H). ^{13}C NMR (DMSO-d_6) δ:

160.1, 154.9, 152.5, 151.0, 149.3, 147.9, 131.9, 129.6, 125.6, 122.8, 121.1, 116.3, 115.5, 114.4, 111.6, 106.4, 77.3, 27.9.

HRMS (ESI): *m/z* 363.1352 [M + H] +; calcd. for $C_{21}H_{19}N_2O_4$, 363.1345

(E)-N'-(2-hydroxy-3-methoxybenzylidene)-7,7-dimethyl-7H-furo[2,3-f]chromene-2-carbohydrazide (11m)

Yield: 75%. M.p.: 215-216 °C; IR (ATR), cm^{-1}: 3265, 1670, 1640, 1603, 1588, 1539, 1463, 1358, 1300, 1265, 1252, 1194, 1156, 1114, 1061, 729.

^1H NMR (DMSO-d_6) δ: 12.09 (s, 1H, NH), 10.63 (s, 1H, OH), 8.71 (s, 1H, CH=N), 7.61 (s, 1H), 7.50 (d, 1H, *J* = 8.8 Hz), 7.17 (d, 1H, *J* = 7.6 Hz), 7.02 (d, 1H, *J* = 7.6 Hz), 6.85 (d, 1H, *J* = 10.0 Hz), 6.84 (t, 1H, *J* = 7.6), 6.80 (d, 1H, *J* = 8.8 Hz), 5.91 (d, 1H, *J* = 10.0 Hz), 3.79 (s, 3H), 1.41 (s, 6H). ^{13}C NMR (DMSO-d_6) δ: 154.9, 152.6, 151.2, 148.6, 148.5, 147.6, 147.4, 131.9, 123.0, 121.1, 120.8, 119.7 (×2), 115.4, 114.5, 114.4, 112.2, 106.4, 77.4, 56.4, 27.9.

HRMS (ESI): *m/z* 393.1467 [M + H] +; calcd. for $C_{22}H_{21}N_2O_5$, 393.1450

(E)-N'-(2-hydroxy-4-methoxybenzylidene)-7,7-dimethyl-7H-furo[2,3-f]chromene-2-carbohydrazide (11n)

Yield: 72%. M.p.: 165-167 °C; IR (ATR), cm^{-1}: 3157, 1644, 1589, 1529, 1489, 1265, 1198, 1163, 1113, 1062, 1031, 727.

^1H NMR (DMSO-d_6) δ: 12.09 (s, 1H, NH), 10.40 (s, 1H, OH), 8.68 (s, 1H, CH=N), 7.62 (s, 1H), 7.50 (d, 1H, *J* = 8.4 Hz), 7.13 (d, 1H, *J* = 2.8 Hz), 6.90 (dd, 1H, *J* = 8.8, 2.8 Hz), 6.85 (d, 1H, *J* = 10.0 Hz), 6.84 (d, 1H, *J* = 8.8 Hz), 6.80 (d, 1H, *J* = 8.4 Hz), 5.90 (d, 1H, *J* = 10.0 Hz), 3.71

(s, 3H), 1.41 (s, 6H). ^{13}C NMR (DMSO-d_6) δ: 155.0, 152.7, 152.6, 151.9, 151.2, 148.0, 147.4, 131.9, 123.0, 121.1, 119.7, 119.0, 117.8, 115.4, 114.5, 112.2, 112.1, 106.4, 77.4, 56.0, 27.9,

HRMS (ESI): m/z 393.1220 [M + H] +; calcd. for $C_{22}H_{21}N_2O_5$, 393.1450

(E)-N'-(2-hydroxy-5-methoxybenzylidene)-7,7-dimethyl-7H-furo[2,3-f]chromene-2-carbohydrazide (11o)

Yield: 88%. M.p.: 180-182 °C; IR (ATR), cm^{-1}: 3494, 3224, 1624, 1602, 1590, 1507, 1485, 1472, 1363, 1343, 1269, 1227, 1201, 1160, 1114, 1068, 1025, 836, 738.

^{1}H NMR (DMSO-d_6) δ: 12.02 (s, 1H, OH), 11.36 (s, 1H, NH), 8.60 (s, 1H, CH=N), 7.59 (s, 1H), 7.49 (d, 1H, *J* = 8.4 Hz), 7.44 (d, 1H, *J* = 8.4 Hz), 6.85 (d, 1H, *J* = 10.0 Hz), 6.80 (d, 1H, *J* = 8.4 Hz), 6.51 (dd, 1H, *J* = 8.4, 2.4 Hz), 6.47 (d, 1H, *J* = 2.4 Hz), 5.90 (d, 1H, *J* = 10.0 Hz), 3.75 (s, 3H), 1.41 (s, 6H). ^{13}C NMR (DMSO-d_6) δ: 162.8, 159.9, 154.7, 152.6, 151.1, 149.4, 147.5, 131.9, 131.3, 122.9, 121.1, 115.4, 114.5, 112.4, 112.0, 107.1, 106.4, 101.7, 77.4, 55.9, 27.9.

HRMS (ESI): *m/z* 393.1382 [M + H] +; calcd. for $C_{22}H_{21}N_2O_5$, 393.1450

(E)-N'-(2-hydroxy-5-methylbenzylidene)-7,7-dimethyl-7H-furo[2,3-f]chromene-2-carbohydrazide (11p)

Yield: 35%. M.p.: 195-197 °C; IR (ATR), cm^{-1}: 3227, 3052, 1639, 1626, 1580, 1557, 15291481, 1353, 1274, 1210, 1192, 1156, 1110, 1062, 723.

^{1}H NMR (DMSO-d_6) δ: 12.10 (s, 1H, NH), 10.77 (s, 1H, OH), 8.65 (s, 1H, CH=N), 7.62 (s, 1H), 7.50 (d, 1H, *J* = 8.0 Hz), 7.38 (s, 1H), 7.09 (d, 1H, *J* = 8.0 Hz), 6.86 (d, 1H, *J* = 10.0 Hz), 6.81 (d, 2H, *J* = 8.0 Hz), 5.91 (d, 1H, *J* = 10.0 Hz), 2.23 (s, 3H), 1.41 (s, 6H). ^{13}C NMR (DMSO-d_6)

δ: 155.7, 154.9, 152.6, 151.2, 148.6, 147.4, 132.8, 131.9, 129.3, 128.5, 123.0, 121.1, 119.1, 116.8, 115.4, 114.5, 112.2, 106.4, 77.4, 27.9, 20.5.

HRMS (ESI): *m/z* 377.1516 [M + H] +; calcd. for $C_{22}H_{21}N_2O_4$, 377.1501

(E)-N'-(2-hydroxy-4,6-dimethoxybenzylidene)-7,7-dimethyl-7H-furo[2,3-f]chromene-2-carbohydrazide (11q)

Yield: 62%. M.p.: 219-221 °C; IR (ATR), cm^{-1}: 3179, 1624, 1590, 1484, 1331, 1268, 1212, 1158, 1113, 1097, 1065, 1044, 724.

^1H NMR (DMSO-d_6) δ: 12.26 (s, 1H, OH), 12.11 (s, 1H, NH), 8.87 (s, 1H, CH=N), 7.58 (s, 1H), 7.49 (d, 1H, *J* = 8.4 Hz), 6.85 (d, 1H, *J* = 10.0 Hz), 6.80 (d, 1H, *J* = 8.4 Hz), 6.13 (s, 1H), 6.12 (s, 1H), 5.91 (d, 1H, *J* = 10.0 Hz), 3.82 (s, 3H), 3.76 (s, 3H), 1.41 (s, 6H). ^{13}C NMR (DMSO-d_6) δ: 163.9, 161.4, 160.1, 154.5, 152.6, 151.1, 147.3, 146.8, 131.9, 123.0, 121.1, 115.4, 114.5, 112.1, 106.4, 101.1, 94.4, 91.1, 77.4, 56.5, 56.0, 27.9.

HRMS (ESI): *m/z* 423.0674 [M + H] +; calcd. for $C_{23}H_{23}N_2O_6$, 423.1556

(E)-N'-(3-hydroxy-4-methoxybenzylidene)-7,7-dimethyl-7H-furo[2,3-f]chromene-2-carbohydrazide (11r)

Yield: 67%. M.p.: 186-188 °C; IR (ATR), cm^{-1}: 3480, 3213, 1638, 1605, 1518, 1478, 1439, 1280, 1253, 1210, 1156, 1112, 1062, 737.

^1H NMR (DMSO-d_6) δ: 11.71 (s, 1H, NH), 9.33 (s, 1H, OH), 8.32 (s, 1H, CH=N), 7.57 (s, 1H), 7.48 (d, 1H, *J* = 8.4 Hz), 7.25 (s, 1H), 7.05 (d, 1H, *J* = 8.4 Hz), 6.96 (d, 1H, *J* = 8.4 Hz), 6.86 (d, 1H, *J* = 10.0 Hz), 6.80 (d, 1H, *J* = 8.4 Hz), 5.91 (d, 1H, *J* = 10.0 Hz), 3.78 (s, 3H), 1.41 (s,

6H). ^{13}C NMR (DMSO-d_6) δ: 155.0, 152.5, 151.0, 150.5, 149.1, 147.8, 147.5, 131.9, 127.5, 122.9, 121.1, 121.0, 115.5, 114.4, 112.8, 112.4, 111.6, 106.4, 77.4, 56.1, 27.9.

HRMS (ESI): *m/z* 393.0950 [M + H] +; calcd. for $C_{22}H_{21}N_2O_5$, 393.1450

(E)-N'-(4-hydroxy-3-methoxybenzylidene)-7,7-dimethyl-7H-furo[2,3-f]chromene-2-carbohydrazide (11s)

Yield: 43%. M.p.: 208-209 °C; IR (ATR), cm^{-1}: 3446, 1640, 1594, 1509, 1482, 1427, 1375, 1290, 1265, 1246, 1196, 1156, 1060, 724.

^{1}H NMR (DMSO-d_6) δ: 11.71 (s, 1H, NH), 9.58 (s, 1H, OH), 8.37 (s, 1H, CH=N), 7.57 (s, 1H), 7.47 (d, 1H, *J* = 8.4 Hz), 7.29 (s, 1H), 7.07 (d, 1H, *J* = 8.0 Hz), 6.85 (d, 1H, *J* = 10.0 Hz), 6.83 (d, 1H, *J* = 8.0 Hz), 6.79 (d, 1H, *J* = 8.4 Hz), 5.88 (d, 1H, 6.85 (d, 1H, *J* = 10.0 Hz), 3.81 (s, 3H), 1.39 (s, 6H). ^{13}C NMR (DMSO-d_6) δ: 154.9, 152.5, 151.0, 149.7, 149.6, 148.6, 147.9, 131.9, 126.0, 122.9, 122.8, 121.1, 116.0, 115.5, 114.4, 111.6, 109.5, 106.4, 77.4, 56.1, 27.9.

HRMS (ESI): *m/z* 393.1232 [M + H] +; calcd. for $C_{22}H_{21}N_2O_5$, 393.1450

(E)-N'-(4-hydroxy-3,5-dimethoxybenzylidene)-7,7-dimethyl-7H-furo[2,3-f]chromene-2-carbohydrazide (11t)

Yield: 81%. M.p.: >250 °C; IR (ATR), cm^{-1}: 3211, 1624, 1585, 1536, 1508, 1325, 1270, 1199, 1156, 1110, 1098, 1066, 1057, 728.

^{1}H NMR (DMSO-d_6) δ: 11.76 (s, 1H, NH), 8.95 (s, 1H, OH), 8.36 (s, 1H, CH=N), 7.58 (s, 1H), 7.48 (d, 1H, *J* = 8.4 Hz), 6.97 (s, 2H), 6.85 (d, 1H, *J* = 10.0 Hz), 6.79 (d, 1H, *J* = 8.4 Hz), 5.90 (d, 1H, *J* = 10.0 Hz), 3.80 (s, 6H), 1.40 (s, 6H). ^{13}C NMR (DMSO-d_6) δ: 155.0, 152.5, 151.0,

149.7, 148.7, 147.8, 138.7, 131.9, 124.8, 122.9, 121.1, 115.5, 114.4, 111.7, 106.4, 105.3, 77.4, 56.6, 27.9.

HRMS (ESI): *m/z* 423.1567 [M + H] +; calcd. for $C_{23}H_{23}N_2O_6$, 423.1556

(E)-N'-(4-hydroxy-3,5-dimethylbenzylidene)-7,7-dimethyl-7H-furo[2,3-f]chromene-2-carbohydrazide (11u)

Yield: 81%. M.p.: 248-249 °C; IR (ATR), cm^{-1}: 3222, 1654, 1630, 1602, 1591, 1530, 1482, 1307, 1272, 1263, 1213, 1193, 1157, 1114, 1063, 727.

^1H NMR (DMSO-d_6) δ: 11.69 (s, 1H, NH) 8.77 (s, 1H, OH), 8.29 (s, 1H, CH=N), 7.56 (s, 1H), 7.47 (d, 1H, *J* = 8.4 Hz), 7.29 (s, 2H), 6.86 (d, 1H, *J* = 10.0 Hz), 6.79 (d, 1H, *J* = 8.4 Hz), 5.89 (d, 1H, *J* = 10.0 Hz), 2.18 (s, 6H), 1.40 (s, 6H). ^{13}C NMR (DMSO-d_6) δ: 156.2, 154.9, 152.4, 151.0, 149.4, 147.9, 131.9, 128.1, 125.6, 125.2, 122.8, 121.1, 115.5, 114.4, 111.5, 106.4, 77.3, 27.9, 17.1.

HRMS (ESI): *m/z* 391.1677 [M + H] +; calcd. for $C_{23}H_{23}N_2O_4$, 391.1658

(E)-N'-(4-hydroxy-3-methoxy-5-nitrobenzylidene)-7,7-dimethyl-7H-furo[2,3-f]chromene-2-carbohydrazide (11v)

Yield: 96%. M.p.: > 250 °C; IR (ATR), cm^{-1}: 3524, 1646, 1619, 1580, 1533 1486, 1330, 1276, 1201, 1162, 1117, 1067, 648.

^1H NMR (DMSO-d_6) δ: 11.98 (s, 1H, NH), 8.41 (s, 1H, CH=N), 7.74 (d, 1H, *J* = 1.6 Hz), 7.61 (s, 1H), 7.57 (d, 1H, J = 1.6 Hz), 7.49 (d, 1H, *J* = 8.4 Hz), 6.84 (d, 1H, *J* = 10.0 Hz), 6.80 (d, 1H, *J* = 8.4 Hz), 5.90 (d, 1H, *J* = 10.0 Hz), 3.93 (s, 3H), 1.40 (s, 6H). ^{13}C NMR (DMSO-d_6) δ:

155.2, 152.6, 151.1, 150.5, 147.6, 147.3, 145.2, 137.6, 131.9, 125.1, 123.0, 121.1, 117.0, 115.4, 114.5, 112.4, 112.1, 106.4, 77.4, 57.2, 27.9.

HRMS (ESI): *m/z* 438.1416 [M + H] +; calcd. for $C_{22}H_{20}N_3O_7$, 438.1301

(E)-N'-(3-bromo-4-hydroxy-5-methoxybenzylidene)-7,7-dimethyl-7H-furo[2,3-f]chromene-2-carbohydrazide (11w)

Yield: 74%. M.p.: 246-248 °C; IR (ATR), cm^{-1}: 3524, 3257, 1641, 1584, 1538, 1497, 1483, 1417, 1386, 1302, 1286, 1264, 1201, 1154, 1112, 1064, 1046, 727.

^{1}H NMR (DMSO-d_6) δ: 11.86 (s, 1H, NH), 10.04 (s, 1H, OH), 8.33 (s, 1H, CH=N), 7.59 (s, 1H, 7.49 (d, 1H, *J* = 8.4 Hz), 7.41 (d, 1H, *J* = 1.6 Hz), 7.31 (d, 1H, *J* = 1.6 Hz), 6.85 (d, 1H, *J* = 10.0 Hz), 6.80 (d, 1H, *J* = 8.4 Hz), 5.90 (d, 1H, *J* = 10.0 Hz), 3.88 (s, 3H), 1.40 (s, 6H). ^{13}C NMR (DMSO-d_6) δ: 155.1, 152.5, 151.1, 149.2, 147.9, 147.7, 146.5, 131.9, 127.0, 125.1, 122.9, 121.1, 115.5, 114.5, 111.8, 109.9, 108.7, 106.4, 77.4, 56.8, 27.9.

HRMS (ESI): *m/z* 472.9720 [M + H] +; calcd. for $C_{22}H_{20}{}^{81}BrN_2O_5$, 473.0555

(E)-N'-(4-hydroxy-3-iodo-5-methoxybenzylidene)-7,7-dimethyl-7H-furo[2,3-f]chromene-2-carbohydrazide (11x)

Yield: 61%. M.p.: 237-238 °C; IR (ATR), cm^{-1}: 3511, 3196, 1640, 1585, 1525, 1485, 1411, 1383, 1360, 1265, 1211, 1196, 1157, 1111, 1063, 1044, 725.

^{1}H NMR (DMSO-d_6) δ: 11.84 (s, 1H, NH), 10.08 (s, 1H, OH), 8.31 (s, 1H, CH=N), 7.59 (s, 1H), 7.58 (d, 1H, *J* = 1.6 Hz), 7.49 (d, 1H, *J* = 8.4 Hz), 7.31 (d, 1H, *J* = 1.6 Hz), 6.85 (d, 1H, *J* = 10.0 Hz), 6.80 (d, 1H, *J* = 8.4 Hz), 5.90 (d, 1H, *J* = 10.0 Hz), 3.86 (s, 3H), 1.41 (s, 6H). ^{13}C NMR

(DMSO-d_6) δ: 155.0, 152.5, 151.1, 149.1, 147.9(x2), 147.7, 131.9, 130.9, 127.9, 122.9, 121.1, 115.5, 114.5, 111.8, 109.6, 106.4, 85.0, 77.4, 56.7, 27.9.

HRMS (ESI): *m/z* 519.0421 [M + H] +; calcd. for $C_{22}H_{20}IN_2O_5$, 519.0417

4.3. Chemical and biological based assays

4.3.1. DPPH Free radical scavenging activity

Solutions of furanochromene phenylhydrazones (**11a-11z**) and the positive controls ascorbic acid and Trolox were prepared in methanol at concentrations ranging from 5000-19.5 μM. Test solutions (5 μL) were added to 96 well plates, followed by 2,2-diphenyl-1-picrylhydrazyl (DPPH) radical solution (0.004% in methanol, 245 μL). The plates were placed in a dark cupboard for 30 minutes, followed by measuring the absorbance at 515 nm using a microplate reader. For the control sample methanol (5 μL) was used instead of the test samples. To correct for background absorbance, blank samples were prepared by using 250 μL of methanol. All experiments were carried out in triplicate.

Prior to determining IC_{50} values, the percent scavenging activity at each concentration was calculated using the following equation:

$$\%\text{Scavenging activity} = \frac{A_{control} - A_{sample}}{A_{control}} \times 100$$

$A_{control}$ = average absorbance of DPPH solution without sample or standard; A_{sample} = average absorbance of test sample after 30 min. Data are expressed as the mean value ± standard deviation (S.D.).

4.3.2. CUPRAC assay

The method developed by Apak[52] was used to determine the Cu (II) ion reducing capacity. Test samples were prepared in test tubes, with each tube containing 1 mL each of H_2O, 1 M aqueous ammonium acetate, 10 mM aqueous $CuCl_2$, and 7.5 mM neocuproine in absolute ethanol. An additional 100 µL of solution was added consisting of water only or a combination of water and stock solutions (5 mM in ethanol)* of test samples (TS) as follows: Tube 1, Blank (100 µL H_2O); Tube 2 (10 µL TS, 90 µL H_2O); Tube 3 (20 µL TS, 80 µL H_2O); Tube 4 (30 µL TS, 70 µL H_2O); Tube 5 (40 µL TS, 60 µL H_2O); Tube 6 (50 µL TS, 50 µL H_2O). The final concentration of test samples in the assay mixture ranged from 12.2-60.9 µM. Trolox was used as a positive control. The samples were vortexed for 30 seconds, covered and allowed to sit at room temperature for 30 minutes, before reading the absorbance at 450 nm. Each concentration was set up in triplicate, and the average absorbance values were used to generate the calibration plots. The Trolox Equivalent Antioxidant Capacity (TEAC) coefficient for the assay was determined by relating the molar absorptivity, Ɛ (obtained from the slopes of the calibration plots), of the test samples to that of Trolox as follows: Ɛ Test samples/ Ɛ Trolox. Data are expressed as the mean value ± standard deviation (S.D.).

*Acetonitrile was used for a few of the samples that were not soluble in absolute ethanol.

4.3.3. Inhibition of erastin-induced ferroptosis

Erastin-induced ferroptosis was characterized by measuring the cell viability of HaCaT cells using the tetrazolium MTT assay.[63-64] Briefly, HaCaT cell were seeded in 96-well plates at 1.0×10^4 cells per well and allowed to attach overnight. Then cells were incubated with test compounds for 4 h, followed by an incubation with erastin (20 µM) for 24 h. Next, the MTT reagent (110 µL) was added in each well and incubated for 4 h. Then medium in each well was

removed and the formazan product was dissolved in DMSO (80 μL). The absorbance of each well was recorded using a SpectraMax M2 plate reader (Molecular Devices, Sunnyvale, CA, USA). Statistical analyses were performed using GraphPad Prism 8 (GraphPad Software, La Jolla, CA, USA). Data are expressed as the mean value ± standard deviation (S.D.) obtained from triplicates of experiments. The significance of differences was determined using a one-way analysis of variance (ANOVA).

4.3.4. DNA cleavage studies

DNA cleavage activity of the phenolic furanochromene hydrazones was carried out by gel electrophoresis using double-stranded circular plasmid DNA, pBR322. The assay medium consisted of DNA (250 ng, 1 μL), copper (II) acetate (10 mM, 2 μL), test samples (10 mM in DMF, 2 μL) and pH 7.2 Tris-HCl buffer (25 mM, 15 μL). The DNA control had DNA only with 19 μL of buffer, while the copper (II) acetate control had DNA and copper (II) acetate with 17 μL of buffer). The solvent control had 2 μL of DMF in place of the test samples. The samples were incubated at 37˚C for 24 hours, followed by the addition of 1X DNA loading dye (5 μL). For the concentration dependence studies with derivative **11h,** samples were incubated for 90 minutes prior to the addition of loading dye. The mixtures were then loaded on 1% agarose for 90 minutes at 90 volts in pH 8 TBE buffer. Gels were stained with GelRed® nucleic acid stain (3X, water) for 15 minutes and visualized at 302 nm using a Western blot imager. Each experiment was performed at least two times.

4.4. Molecular docking studies

The X-ray crystal structure of B-DNA (PDB ID: 1BNA) dodecamer d(CGCGAATTCGCG)$_2$ was obtained from the Protein Data Bank (http://www.rcsb.org/pdb). In order to prepare the DNA for docking, polar hydrogens were added and Kollman charges were assigned. The structures of the phenolic furanochromene hydrazones were generated in Avogadro and subjected to energy optimization using a steepest-descent algorithm, followed by adding polar hydrogens and conversion to pdbqt files using Open Babel software. Docking analyses were carried out using AutoDock Tools version 1.5.6 and AutoDock Vina programs.[65] The grid box included the entire B DNA structure, and nine conformational images were created for each ligand. The output files for the lowest energy conformers were exported to PyMol for display of the 3D structure of the DNA-ligand complexes. 2D interaction diagrams were generated using ProteinsPlus server.

Declaration of competing interest

The authors declare that they have no known competing personal relationships or financial interests related to the work presented in this paper.

Acknowledgements

The authors are thankful to Susquehanna University and University of Rhode Island for funding this work. We are also grateful to Dr. Douglas Collins from Bucknell University for assistance in acquiring high resolution mass spectrometry data.

Supplementary Data

^{1}H NMR, ^{13}C NMR, IR and HRMS spectra of compounds **7-9** and **11a-11x** are available in the supplementary file, together with the DNA-ligand 2D interaction map for compounds **11a-11x**.

REFERENCES

1. Raj V, Lee J. 2H/4H chromenes - a versatile biologically active scaffold. *Front Chem*. 2020;8:263.
2. Costa M, Dias TA, Brito A, Proença, F. Biological importance of structurally diversified chromenes. *Eur J Med Chem.* 2016;123:487-507.
3. Auranwiwat C, Limtharakul T, Pyne SG, Rattanajak R, Kamchonwongpaisan S. A new xanthone and a biphenyl from the flower and twig extracts of *Garcinia mckeaniana*. *Nat Prod Res.* 2021;35:3404-3409.
4. Zhang X, Song Z, Li Y, Wang H, Zhang S, Reid A-M, Lall N, Zhang J, Wang C, Lee D, Xu YOJ, Guo Y. Cytotoxic and antiangiogenetic xanthones inhibiting tumor proliferation and metastasis from *Garcinia xipshuanbannaensis. J Nat Prod.* 2021;84:1515-1523.
5. Liu X-J, Hu X, Peng X-H, Wang Y-T, Huang X-F, Zan Y-H, Li D-H, Li Z-L, Hua H-M. Polyprenylated xanthones from the twigs and leaves of *Garcinia nujiangensis* and their cytotoxic evaluation. *Bioorg Chem*. 2020;94:103370.
6. Chen L, Tang G-H, Guo F-L, Li W, Zhang J-S, Liu B, Yin S. (*P*)/(*M*)-corinepalensin A, a pair of axially chiral prenylated bicoumarin enantiomers with a rare C-5-C-5′linkage from the twigs of *Coriaria nepalensis*. *Phytochemistry*. 2018;149:140-145.
7. Fobofou SAT, Franke K, Porzel A, Brandt W, Wessjohann LA. Tricyclic acylphloroglucinols from *Hypericum lanceolatum* and regioselective synthesis of selancins A and B. *J Nat Prod.* 2016;79:743-753.
8. Beniddir MA, Borgne EL, Iorga BI, Loaëc N, Lozach O, Meijer L, Awang K, Litaudon M. Acridone alkaloids from *Glycosmis chlorosperma* as DYRK1A inhibitors. *J Nat Prod.* 2014;77:1117-1122.

9. Manning K, Petrunak E, Lebo M, González-Sarrías A, Seeram NP, Henry GE. Acylphloroglucinol and xanthones from *Hypericum ellipticum. Phytochemistry.* 2011;72:662-667.
10. Mir MA, Mehra U, Sheikh BA. Recent advances in chemotherapeutic implications of deguelin: A plant-derived retinoid. *Nat Prod J.* 2020;10:1-13.
11. Kashman Y, Gustafson KR, Fuller RW, Cardellina JH, McMahon JB, Currens MJ, Buckheit RW Jr, Hughes SH, Cragg GM, Boyd MR. The calanolides, a novel HIV-inhibitory class of coumarin derivatives from the Tropical Rainforest tree, *Calophyllum lanigereum. J Med Chem*. 1992;35:2735-2743.
12. Nahar L, Talukdar AD, Nath D, Nath S, Mehan A, Ismail FMD, Sarker SD. Naturally occurring calanolides: Occurrence, biosynthesis, and pharmacological properties including therapeutic potential. *Molecules.* 2020;25:4983.
13. Lee J-E, Bo F, Thuy NTT, Hong J, Lee JS, Cho N, Yoo HM. Anticancer activity of lesbicoumestan in Jurkat cells via inhibition of oxidative stress-mediated apoptosis and MALT1 protease. *Molecules*. 2021;26:185.
14. Thuy NTT, Lee J-E, Yoo HM, Cho N. Antiproliferative pterocarpans and coumestans from *Lespedeza bicolor*. *J Nat Prod*. 2019;82:3025-3032.
15. Malaník M, Treml J, Leláková V, Nykodýmová D, Oravec M, Marek J, Šmejkal K. Anti-inflammatory and antioxidant properties of chemical constituents of *Broussonetia papyrifera. Bioorg Chem*. 2020;104:104298.
16. Kapche GDWF, Fozing CD, Donfack JH, Fotso GW, Amadou D, Tchana AN, Bezabih M, Moundipa PF, Ngadjui BT, Abegaz BM. Prenylated arylbenzofuran derivatives from *Morus mesozygia* with antioxidant activity. *Phytochemistry.* 2009;70:216-221.

17. Naik R, Harmalkar DS, Xu X, Jang K, Lee K. Bioactive benzofuran derivatives: moracins A-Z in medicinal chemistry. *Eur J Med Chem*. 2015;90:379-393.
18. Paudel P, Seong SH, Zhou Y, Ha MT, Min BS, Jung HA, Choi JS. Arylbenzofurans from the root bark of *Morus alba* as triple inhibitors of cholinesterase, β-site amyloid precursor protein cleaving enzyme 1, and glycogen synthase kinase-3β: Relevance to Alzheimer's disease. *ACS Omega*. 2019;4:6283-6294.
19. Chan EWC, Wong SK, Tangah J, Inoue T, Chan HT. Phenolic constituents and anticancer properties of *Morus alba* (white mulberry) leaves. *J Integr Med.* 2020;18:189-195.
20. Nguyen C-T, Ann J, Sahu R, Byun WS, Lee S, Nam G, Park H-J, Park S, Kim Y-J, Kim JY, Seo JH, Lee J. Discovery of novel anti-breast cancer agents derived from deguelin as inhibitors of heat shock protein 90 (HS90). *Bioorg Med Chem Lett.* 2020;30:127374.
21. An H, Lee S, Lee JM, Jo DH, Kim J, Jeong Y-S, Heo MJ, Cho CS, Choi H, Seo JH, Hwang S, Lim J, Kim T, Jun HO, Sim J, Lim C, Hur J, Ahn J, Kim HS, Seo S-Y, Na Y, Kim S-H, Lee J, Lee J, Chung S-J, Kim Y-M, Kim K-W, Kim SG, Kim JH, Suh Y-G. Novel hypoxia-inducible factor 1α (HIF-1α) inhibitors for angiogenesis-related ocular diseases: Discovery of a novel scaffold via ring-truncation strategy. *J Med Chem.* 2018;61:9266-9286.
22. Liu Z, Guo X, Liu G. Modified calanolides incorporated with furan-2-nitro mimics against *Mycobacterium tuberculosis*. *Bioorg Med Chem Lett*. 2015;25:1297-1300.
23. Ma T, Liu L, Xue H, Li L, Han C, Wang L, Chen Z, Liu G. Chemical library and structure-activity relationships of 11-demethyl-12-oxo calanolide A analogues as anti-HIV-1 agents. *J Med Chem*. 2008;51:1432-1446.

24. Singh S, Agarwal K, Iqbal H, Yadav P, Yadav D, Chanda D, Tandon S, Khan F, Gupta AK, Gupta A. Synthesis and evaluation of substituted 8,8-dimethyl-8H-pyrano[2,3-f]chromen-2-one derivatives as vasorelaxing agents. *Bioorg Med Chem Lett*. 2020;30:126759.

25. Azevedo CMG, Afonso CMM, Soares JX, Reis S, Sousa D, Lima RT, Vasconcelos MH, Pedro M, Barbosa J, Gales L, Pinto MMM. Pyranoxanthones: Synthesis, growth inhibitory activity on human tumor cell lines and determination of their lipophilicity in two membrane models. *Eur J Med Chem.* 2013;69:798-816.

26. Seo Y, Choi J, Lee JH, Kim TG, Park S, Han G, Namkung W, Kim I. Diversity-oriented generation and biological evaluation of new chemical scaffolds bearing a 2,2-dimethyl-2H-chromene unit: Discovery of novel potent ANO1 inhibitors. *Bioorg Chem*. 2020;101:104000.

27. Boddupally S, Jyothi P, Rao MVB, Rao KP. Design and synthesis of antimicrobial active (E)-(3-(Substituted-styryl)- 7H-furo[2,3-f]chromen-2-yl)(phenyl)methanone derivatives and their in silico molecular docking studies. *J Heterocycl Chem*. 2019;56:73-80.

28. Ashok D, Rangu K, Gundu S, Rao V. Synthesis of pyrazolylfuro[2,3-*f*]chromenes and evaluation of their antimicrobial activity. *Chem Heterocycl Comp.* 2016;52**:**928-933.

29. Pisoschi AM, Pop A, Iordache F, Stanca L, Predoi G, Serban AI. Oxidative stress mitigation by antioxidants - An overview on their chemistry and influences on health status. *Eur J Med Chem*. 2021;209:112891.

30. Tan BL, Norhaizan ME, Liew W-P-P, Rahman HS. Antioxidant and oxidative stress: A mutual interplay in age-related diseases. *Front Pharmacol*. 2018;9:1162.

31. Yuan H, Pratte J, Giardina C. Ferroptosis and its potential as a therapeutic target. *Biochem Pharmacol.* 2021;186:114486.
32. Haider K, Haider MR, Neha K, Yar MS. Free radical scavengers: An overview on heterocyclic advances and medicinal prospects. *Eur J Med Chem*. 2020;204:112607.
33. Nimse SB, Pal D. Free radicals, natural antioxidants, and their reaction mechanisms. *RSC Adv.* 2015;5:27986-28006.
34. Lesjak M, Simin N, Srai SKS. Can polyphenols inhibit ferroptosis? *Antioxidants*. 2022;11:150.
35. Kajarabille N, Latunde-Dada GO. Programmed cell-death by ferroptosis: Antioxidants as mitigators. *Int J Mol Sci.* 2019;20:4968.
36. da Silva DA, De Luca A, Squitti R, Rongioletti M, Rossi L, Machado CML, Cerchiaro G. Copper in tumors and the use of copper-based compounds in cancer treatment. *J Inorg Biochem.* 2022;226:111634.
37. Jomová K, Hudecova L, Lauro P, Simunkova M, Alwasel SH, Alhazza IM, Valko M. A Switch between antioxidant and prooxidant properties of the phenolic compounds myricetin, morin, 3',4'-dihydroxyflavone, taxifolin and 4-hydroxy-coumarin in the presence of copper(II) Ions: A spectroscopic, absorption titration and DNA damage study. *Molecules.* 2019;24:4335.
38. Farhan M, Oves M, Chibber S, Hadi SM, Ahmad A. Mobilization of nuclear copper by green tea polyphenol epicatechin-3-gallate and subsequent prooxidant breakage of cellular DNA: Implications for cancer chemotherapy. *Int J Mol Sci.* 2017;18:34.

39. Cherrak SA, Mokhtari-Soulimane N, Berroukeche F, Bensenane B, Cherbonnel A, Merzouk H, Elhabiri, M. In vitro antioxidant versus metal ion chelating properties of flavonoids: A structure-activity investigation. *PLoS ONE.* 2016;11:0165575.

40. Kumar HMS, Herrmann L, Tsogoeva SB. Structural hybridization as a facile approach to new drug candidates. *Bioorg Med Chem Lett*. 2020;30:127514.

41. Shah SK, Goyal A. A review for biological activity on hydrazide hydrazones: A promising moiety. *Eur J Mol Clin Med*. 2020;7:857-881.

42. Wahbeh J, Milkowski S. The use of hydrazones for biomedical applications. *SLAS Technol.* 2019;24:161-168.

43. Thota S, Rodrigues DA, Pinheiro PSM, Lima LM, Fraga CAM, Barreiro EJ. N-Acylhydrazones as drugs. *Bioorg Med Chem Lett*. 2018;28:2797-2806.

44. Patil S, Kuman MM, Palvai S, Sengupta P, Basu S. Impairing powerhouse in colon cancer cells by hydrazide-hydrazone-based small molecule. *ACS Omega.* 2018;3:1470-1481.

45. Baldisserotto A, Demurtas M, Lampronti I, Tacchini M, Moi D, Balboni G, Vertuani S, Manfredini S, Onnis V. In-vitro evaluation of antioxidant, antiproliferative and photo-protective activities of benzimidazole hydrazone derivatives. *Pharmaceuticals.* 2020;13:68.

46. Demurtas M, Baldisserotto A, Lampronti I, Moi D, Balboni G, Pacifico S, Vertuani S, Manfredini S, Onnis V. Indole derivatives as multifunctional drugs: Synthesis and evaluation of antioxidant, photoprotective and antiproliferative activity of indole hydrazones. *Bioorg Chem*. 2019;85:568-576.

47. Baldisserotto A, Demurtas M, Lampronti I, Moi D, Balboni G, Vertuani S, Manfredini S, Onnis V. Benzofuran hydrazones as potential scaffold in the development of multifunctional drugs: Synthesis and evaluation of antioxidant, photoprotective and antiproliferative activity. *Eur J Med Chem*. 2018;156:118-125.
48. Cui Z, Li Y, Ling Y, Huang J, Cui J, Wang R, Yang X. New class of potent antitumor acylhydrazone derivatives containing furan. *Eur J Med Chem.* 2010;45:5576-5584.
49. Moussa Z, Al-Mamary M, Al-Juhani S. Ahmed SA. Preparation and biological assessment of some aromatic hydrazones derived from hydrazides of phenolic acids and aromatic aldehydes. *Heliyon*. 2020;6:e050192.
50. Bino A, Baldisserotto A, Scalambra E, Dissette V, Vedaldib DE, Salvador A, Durini E, Manfredini S, Vertuani S. Design, synthesis and biological evaluation of novel hydroxy-phenyl-1H-benzimidazoles as radical scavengers and UV-protective agents. *J Enzyme Inhib Med Chem.* 2017;32:527-537.
51. Mathew S, Abraham TE, Zakaria ZA. Reactivity of phenolic compounds towards free radicals under in vitro conditions. *J Food Sci Technol*. 2015;52:5790-5798.
52. Özyürek M, Güclü K, Tütem E, Başkan KS, Erçağ E, Çelik SE, Baki S, Yildiz L, Karaman S, Apak R. A comprehensive review of CUPRAC methodology. *Anal Methods.* 2011;3:2439-2453.
53. Apak R, Güçlü K, Demirata B, Özyürek M, Çelik SE, Bektaşoğlu B, Berker KI, Özyurt D. Comparative evaluation of various total antioxidant capacity assays applied to phenolic compounds with the CUPRAC assay. *Molecules*. 2007;12:1496-1547.

54. Cheng J, Xu T, Xun C, Guo H, Cao R, Gao S, Sheng W. Carnosic acid protects against ferroptosis in PC12 cells exposed to erastin through activation of Nrf2 pathway. *Life Sci.* 2021;266:118905.

55. Simultaneous study of anti-ferroptosis and antioxidant mechanisms of butein and (S)-butin. *Molecules*. 2020;25:674.

56. Li X, Zeng J, Liu Y, Liang M, Liu Q, Li Z, Zhao X, Chen D. Inhibitory effect and mechanism of action of quercetin and quercetin Diels-Alder anti-dimer on erastin-induced ferroptosis in bone marrow-derived mesenchymal stem cells. *Antioxidants*. 2020;9:205.

57. Kose T, Vera-Aviles M, Sharp PA, Latunde-Dada GO. Curcumin and (−)-Epigallocatechin-3-Gallate Protect Murine MIN6 Pancreatic Beta-Cells Against Iron Toxicity and Erastin-Induced Ferroptosis. *Pharmaceuticals*. 2019;12:26.

58. Elmegerhi S, Su C, Buglewicz DJ, Aizawa Y, Kato TA. Effect of hydroxyl group position in flavonoids on inducing single-stranded DNA damage mediated by cupric ions. *Int J Mol Med.* 2018;42:658-664.

59. Asmita D, Debashis M, Chabita S. Correlation of binding efficacies of DNA to flavonoids and their induced cellular damage. *J Photochem Photobiol B, Biol.* 2017;170:256-262.

60. Neidle S. Beyond the double helix: DNA structural diversity and the PDB. *J Biol Chem*. 2021;296:100553.

61. Bilge S, Dogan-Topal B, Tok TT, Atici EB, Sınağ A, Ozkan SA. Investigation of the interaction between anticancer drug ibrutinib and double-stranded DNA by electrochemical and molecular docking techniques. *Microchem J.* 2022;180:107622.

62. Henry GE, Jacobs H. A short synthesis of 5-methoxy-2,2-dimethyl-2*H*-benzopyran-6-propanoic acid methyl ester. *Tetrahedron*. 2001;57:5335-5338.

63. Xie Y, Chen G. Dioscin induces ferroptosis and synergistic cytotoxicity with chemotherapeutics in melanoma cells. *Biochem Biophys Res Commun.* 2021:557:213-220.

64. Ma H, DaSilva NA, Liu W, Nahar PP, Wei Z, Liu Y, Pham PT, Crews R, Vattem DA, Slitt AL, Shaikh ZA, Seeram NP. Effects of a standardized phenolic-enriched maple syrup extract on β-amyloid aggregation, neuroinflammation in microglial and neuronal cells, and β-amyloid induced neurotoxicity in *Caenorhabditis elegans. Neurochem Res.* 2016;42:2836-2847.

65. Trott O, Olson AJ. AutoDock Vina: improving the speed and accuracy of docking with a new scoring function, efficient optimization and multithreading. *J Comput Chem.* 2010;31:455-461.